International Journal of Heat and Mass Transfer 148 (2020) 119080

Contents lists available at ScienceDirect

International Journal of Heat and Mass Transfer

journal homepage: www.elsevier.com/locate/hmt

The general supercritical heat transfer correlation for vertical up-flow tubes: *K* number correlation

Bingguo Zhu, Jinliang Xu*, Chenshuai Yan, Jian Xie

The Beijing Key Laboratory of Multiphase Flow and Heat Transfer, North China Electric Power University, Beijing, 102206 Beijing, China

ARTICLE INFO

Article history:
Received 14 August 2019
Revised 17 November 2019
Accepted 19 November 2019

Keywords:
Supercritical heat transfer
Pseudo-boiling
K number
Heat transfer correlation

ABSTRACT

The objective of this paper is to present a general supercritical heat transfer (SHT) correlation for advanced power cycles. In textbooks, supercritical fluid is considered to have single-phase structure. However, various SHT correlations incorporating buoyancy/acceleration effects fail to predict heat transfer coefficients. Here, pseud-boiling assumption is introduced to deal with SHT. Supercritical fluid is treated to have a heterogeneous structure consisting of vapor-like fluid and liquid-like fluid. Similarity analysis between subcritical boiling and SHT creates a new dimensionless parameter, the *K* number, representing evaporation induced momentum force relative to inertia force to govern the growth of wall attached vapor-like fluid layer thickness, which is key to dominate SHT. Thus, SHT is correlated in a simple form as $Nu = CRe_b^{n1}Pr_{b,ave}^{n2}K^{n3}$, where Nu, Re_b, $Pr_{b,ave}$ are Nusselt number, Reynolds number and Prandtl number, respectively. Totally, 5560 data points, including our newly obtained 2028 data points for S-CO_2 with pressures up to 21 MPa, and other 3532 data points cited from 18 articles for carbon dioxide, water and R134a, are used to determine the coefficients C and n1−n3, yielding the expression of$Nu = 0.0012Re_b^{0.9484}Pr_{b,ave}^{0.718}K^{-0.0313}$. The negative exponent −0.0313 for the *K* number explains the improved heat transfer by increasing pressures. By comparing with experiment database, the general correlation has better prediction accuracy than the widely cited correlations in the literature. The correlation is also compared with R22 data. Even though such data are not involved in the development of the SHT correlation, the correlation excellently matched the experimental data. This work paves a new road to understand SHT. The correlation ensures heat exchangers operating at supercritical pressures to be designed more accurately and safely.

1. Introduction

Since Baron Charles Cagniard de la Tour found supercritical fluid in 1822, supercritical fluid attracts researchers to promote its application, including the extraction of floral fragrance from flowers, functional food ingredients, pharmaceuticals, cosmetics, powders, and functional materials [1,2]. All these applications are based on the distinct mass, momentum and energy transfer when crossing the critical or pseudo-critical point. In thermal and power engineering, supercritical fluid converts thermal energy into power. Supercritical Rankine cycle or Brayton cycle have higher efficiencies than subcritical cycle [3]. A vapor-liquid separator is not necessary, which is another benefit to simplify the system design [4]. Recent studies show that S-CO_2 Brayton cycle is more attractive for heat-power conversion than water-steam Rankine cycle, which is expected to be used in Generation IV nuclear reactor [5], solar energy [6] and fossil energy power plant [7]. Organic fluids such as R134a are used in organic Rankine cycle (ORC) for low grade energy extraction [8].

Supercritical heat transfer (SHT) is important to design a supercritical cycle. When crossing pseudo-critical point, heat transfer is either enhanced, called normal heat transfer (NHT), or is deteriorated, called heat transfer deterioration (HTD) [9]. When the fluid is beyond the pseudo-critical point, SHT is just like the convective gas heat transfer. Sometimes, heat transfer coefficients are not as high as one imagines. For an S-CO_2 coal fired power plant, assuming a heat transfer coefficient of 3 kW/m^{2}K, the temperature difference between inner wall and bulk fluid attains 100 K at a heat flux of 300 kW/m^2, which is a challenge to keep the safe operation of an S-CO_2 boiler [10]. Experimental SHT studies have been performed by independent research groups worldwidely. Driven by the development of nuclear reactor and fossil energy power plant, fruitful SHT water data were obtained since 1950s [11]. S-CO_2 cy-

* Corresponding author.
E-mail address: xjl@ncepu.edu.cn (J. Xu).

https://doi.org/10.1016/j.ijheatmasstransfer.2019.119080
0017-9310/

Nomenclature

Ac	flow acceleration parameter
Bu	buoyancy parameter
C	coefficient
c	critical point
c_p	specific heat, J/kg•K
D	bubble diameter, m
d_{in}	inner diameter of the tube, m
e	error
F	force, N
G	mass flux, kg/m^{2}s
Gr	Grashof number
H	a function of several correction terms of physical properties
h	heat transfer coefficient, W/m^{2}K
i	enthalpy, J/kg
Δi	pseudo-boiling enthalpy, J/kg
K	non-dimensional parameter representing evaporation induced momentum force relative to inertia force
k	coefficient referring to pseudo-boiling enthalpy with respect to enthalpy at the pseudo-critical point
L	length, m
M	molar mass, g/mol
m	mass flow rate, kg/s
Nu	Nusselt number
n1−n3	coefficients
P	pressure, Pa
Pr	Prandtl number
Q	heating power, W
q	heat flux, W/m^2
q^+	non-dimensional heat flux
Re	Reynolds number
R	gas constant
R_g	molar gas constant, J/(mol•K)
T	temperature, °C
T^-	the starting temperature of pseudo-boiling, °C
T^+	the ending temperature of pseudo-boiling, °C
ΔT	temperature span from T^- to T^+, °C
t	time
ΔV	volume change, m^3

Greek symbols

β	thermal expansion coefficient, 1/K
γ	specific heat ratio
θ	contact angle, o
λ	heat conductivity coefficient, W/mK
μ	dynamic viscosity, Pa•s
ν	kinematic viscosity, m^2/s
ρ	density, kg/m^3

Subscripts

A	mean relative
ave	average
b	bulk fluid
D−B	Dittus−Bolter
exp	experiment
fg	saturation vapor-liquid
I'	inertia
in	inlet
l	liquid
M'	momentum
out	outlet
pc	pseudo-critical
pre	prediction
R	mean absolute
S	root-mean-square relative
v	vapor
w	inner wall

Acronyms

DNB	departure from nuclear boiling
DC	direct current
HTD	heat transfer deterioration
NHT	normal heat transfer
ORC	organic Rankine cycle
SHT	supercritical heat transfer
S-CO_2	supercritical CO_2
sup	supercritical
sub	subcritical
WL	Widom line

cle is a relatively new concept. Experiment data are insufficient to support key heat exchanger design when using S-CO_2 at this stage. Most of available CO_2 heat transfer studies are focused on narrow data ranges. Especially, experiment data were obtained near the critical pressure ~8 MPa. A practical S-CO_2 cycle may operate the system at pressure up to 20−30 MPa. In this paper, one of the important tasks is to present CO_2 heat transfer data at sufficiently high pressure.

As documented in textbooks [12], a fluid can have vapor/liquid two-phase structure at subcritical pressure. Liquid is converted into vapor at a constant saturation temperature. Latent heat of evaporation i_{fg} quantifies the heat necessary for liquid-vapor phase change per unit mass. Once the pressure is beyond the critical value, a fluid only has the single-phase like structure without vapor-liquid interface. Based on the framework of single-phase fluid at supercritical pressure, the varied physical properties and buoyancy/acceleration effects are believed to cause abnormal heat transfer behavior for more than half century [13]. Recently, various investigations show that SHT correlations based on the buoyancy/acceleration effects are not success to predict supercritical heat transfer [14,15]. Table 1 lists five widely cited correlations [16–20]. SHT correlations can be classified into two categories. The first category correlates Nusselt number as $Nu = CRe_b^{n1}Pr_{b,ave}^{n2}H$, where H is a function of several correction terms of physical properties characterized by inner wall temperature T_w with respect to bulk fluid temperature T_b. The correlations of Bishop et al. [16], Jackson [17], Jackson and Hall [18] and Gupta et al. [19] belong to this category. The other category correlates SHT as $Nu = CRe_b^{n1}Pr_{b,ave}^{n2}Bu^{n3}Ac^{n4}$, where Bu and Ac represent the correction terms of buoyancy effect and acceleration effect, respectively. The Yu et al. [20] correlation belongs to this category.

The literature survey shows that: (i) Some SHT correlations are suitable in their own data range, but cannot be extended for other experiment data [9,21]. (ii) There are no SHT correlations suitable for different working fluids [10]. (iii) There are no SHT correlations which are suitable not only for normal heat transfer, but also for heat transfer deterioration [22]. In summary, the available works emphasize the importance of varied physical properties and buoyancy/acceleration effects on SHT. Huang and Li [23] emphasized the inconsistences of SHT, due to the not properly treated buoyancy effect in the literature.

The objective of this paper is to present a general supercritical heat transfer correlation, based on sufficient experiment database. The framework of single-phase, homogeneous structure of supercritical fluid is abandoned. SHT is analyzed with pseudo-boiling. By linking boiling at subcritical pressure with pseudo-boiling at su-

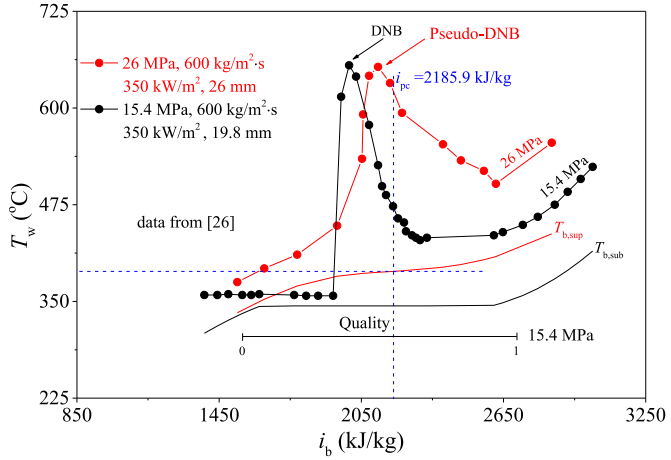

Fig. 1. The analogy regarding heat transfer deterioration at subcritical pressure and supercritical pressure.

percritical pressure, the *K* number is proposed to play a key role on heat transfer coefficient. Except Reynolds number and Prandtl number, the proposed correlation only contains one correction term of the *K* number. The simple expression ensures fast iteration calculation and avoids multi-solutions under given heat flux condition. The correlation is verified to have the highest accuracy among the widely cited correlations in the literature. By comparing the correlation predictions with extended experiment data, the correlation is believed to be general for various working fluids, due to the similarity numbers used for the correlation.

The paper is organized as follows. Section 2 describes the theoretical basis of pseudo-boiling for supercritical heat transfer. Section 3 describes the experimental database and the proposed correlation. Section 4 deals with the results and discussion. Major conclusions are summarized in Section 5.

2. Theoretical basis of pseudo-boiling for supercritical heat transfer

2.1. Evidence of pseudo-boiling at supercritical pressure

Pseudo-boiling was proposed in 1960s. Nishikawa and Miyabe [24] presented photographs of what they considered to be normal boiling and film boiling of supercritical pressure carbon dioxide. They were convinced a boiling-like phenomenon for normal heat transfer, and a film boiling phenomenon for heat transfer deterioration. Ackerman [25] investigated SHT of water. He noted a sudden increase in heat transfer coefficient, attributed to a boiling-like process similar to subcooled nucleate boiling at subcritical pressure, and a sudden decrease in heat transfer coefficient, attributed to a pseudo-boiling process similar to vapor-film boiling at subcritical pressure. Wang et al. [26] observed that both of subcritical pressure and supercritical pressure display similar wall temperature peaks when heat transfer deterioration occurs, corresponding to departure of nucleate boiling (DNB) at subcritical pressure and pseudo-DNB (pseudo-boiling) at supercritical pressure (see Fig. 1). Holman et al. [27] investigated SHT of Freon 12. Photographs were presented for boiling-like flow. The intensity of vapor trails increases at wall temperatures in supercritical range. Stewart et al. [28] studied SHT of water in horizontal tubes. Pressure oscillations were detected, resulting from standing pressure wave propagation between entry and exit of the test section.

Pseudo-boiling infers the co-existence of liquid-like fluid and gas-like fluid at supercritical pressure. Supercritical fluid structure

Table 1
Supercritical heat transfer correlations existed in the literature.

Authors	Correlations	Fluid and parameter range
Bishop et al. [16]	$Nu = 0.0069Re_b^{0.9}Pr_{b,ave}^{0.66}(\frac{\rho_w}{\rho_b})^{0.43}(1+\frac{2.4}{L/d_{in}}), Re_b = \frac{Gd_{in}}{\nu_b}, Pr_{b,ave} = \frac{\mu_b c_{p,ave}}{\lambda_b}, c_{p,ave} = \frac{i_w - i_b}{T_w - T_b}$	H_2O, *P*: 22.6–27.6 MPa, *G*: 651–3662 kg/m²s, q_w: 310–3460 kW/m², d_{in}: 2.54–5.08 mm
Jackson [17]	$Nu = 0.0183Re_b^{0.82}Pr_{b,ave}^{0.5}(\frac{\rho_w}{\rho_b})^{0.3}, Re_b = \frac{Gd_{in}}{\nu_b}, Pr_{b,ave} = \frac{\mu_b c_{p,ave}}{\lambda_b}, c_{p,ave} = \frac{i_w - i_b}{T_w - T_b}$	CO_2, *P*: 7.8–9.8 MPa, *Re*: 8×10^4–5×10^5, q_w≤260 kW/m², d_{in}: 4.1 mm
Jackson and Hall [18]	$Nu = 0.0183Re_b^{0.82}Pr_b^{0.5}(\frac{\rho_w}{\rho_b})^{0.3}(\frac{c_{p,ave}}{c_{p,b}})^n, Re_b = \frac{Gd_{in}}{\nu_b}, Pr_{b,ave} = \frac{\mu_b c_{p,ave}}{\lambda_b}, c_{p,ave} = \frac{i_w - i_b}{T_w - T_b}$ $0.4: T_b < T_w < T_{pc}$ or $1.2T_{pc} < T_b < T_w$ $n = \{0.4 + 0.2(T_w/T_{pc} - 1): T_b < T_{pc} < T_w$ $0.4 + 0.2(\frac{T_w}{T_{pc}} - 1)[1 - 5(\frac{T_b}{T_{pc}} - 1)]: T_{pc} < T_b < 1.2T_{pc}$	CO_2, after review of the existing literatures and data
Gupta et al. [19]	$Nu = 0.01Re_b^{0.89}Pr_{b,ave}^{-0.14}(\frac{\rho_w}{\rho_b})^{0.93}(\frac{\lambda_w}{\lambda_b})^{0.22}(\frac{\mu_w}{\mu_b})^{-1.13}, Pr_{b,ave} = \frac{\mu_b c_{p,ave}}{\lambda_b}, c_{p,ave} = \frac{i_w - i_b}{T_w - T_b}$	CO_2, *P*: 7.57–8.8 MPa, *G*: 706–3167 kg/m²s, q_w: 9.3–616.6 kW/m², d_{in}: 8 mm
Yu et al. [20]	$Nu = 0.0138Re_b^{0.9078}Pr_{b,ave}^{0.6171}(\frac{\rho_w}{\rho_b})^{0.4356}Gr^{-0.012}(q^+)^{0.0605}, Pr_{b,ave} = \frac{\mu_b c_{p,ave}}{\lambda_b}, c_{p,ave} = \frac{i_w - i_b}{T_w - T_b}, Gr = \frac{g\beta_b d_{in}^4 q_w}{\lambda_b \nu_b^2}$, $q^+ = \frac{q_w \beta_b}{G c_p}, \beta_b = -\frac{1}{\rho_b}(\frac{\partial \rho_b}{\partial T_b})_p$	H_2O, *P*: 22.6–41 MPa, *G*: 90–2150 kg/m²s, q_w: 110–1800 kW/m², d_{in}: 1.5–38.1 mm

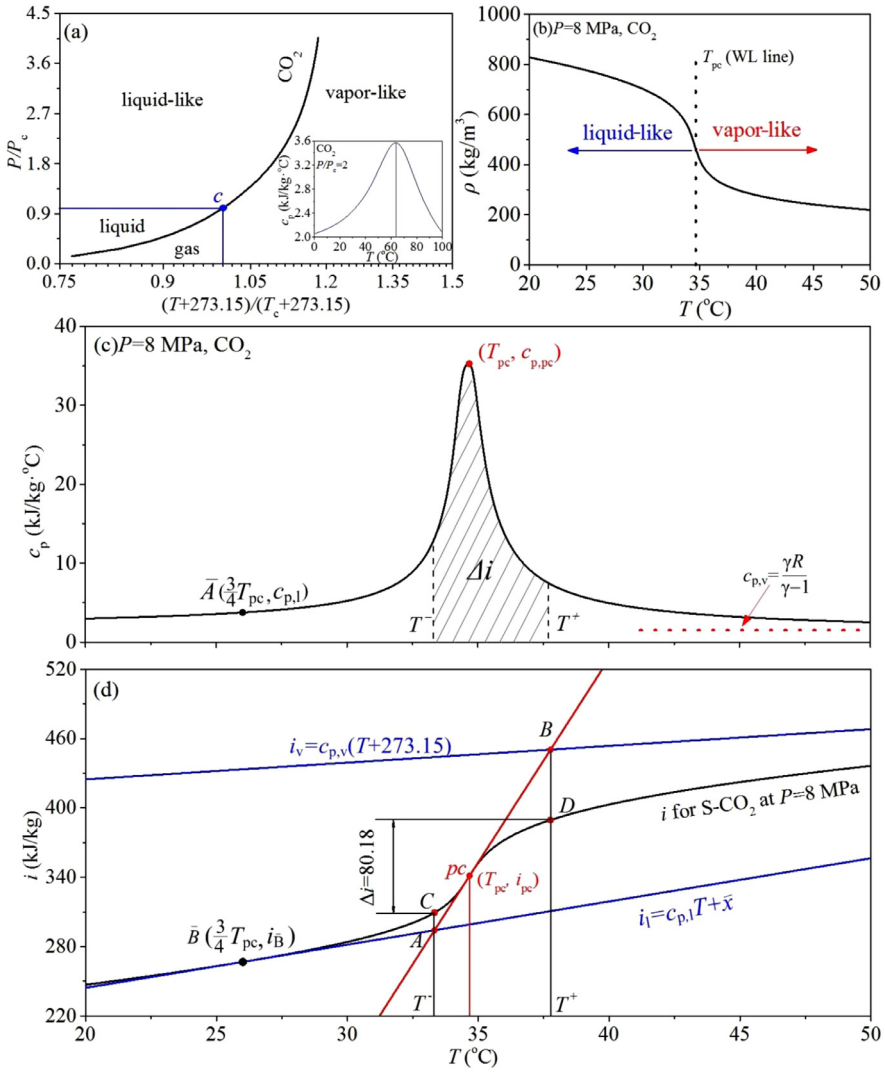

Fig. 2. Thermodynamic behavior at supercritical pressures (a): the $P/P_c-T/T_c$ curve characterizing the transition from liquid to vapor at subcritical pressures and from liquid−like fluid to vapor−like fluid at supercritical pressure; (b): the interface between liquid-like fluid and vapor-like fluid; (c): the c_p curve of CO_2 at P=8 MPa; (d): temperature −enthalpy curve at supercritical pressure to define Δi, T^- and T^+. (For interpretation of the references to color in this figure, the reader is referred to the web version of this article.)

has been received attention by physicists. Simeoni et al. [29] determined the velocity of nanometric acoustic waves in supercritical argon at high pressures by inelastic X-ray scattering and molecular dynamics simulations. A sharp transition on crossing the Widom line demonstrates that supercritical fluid can be identified by different dynamical regimes: gas-like and liquid-like, reminiscent of subcritical domains. Pseudo-boiling was well documented by Banuti [30].

The theoretical basis of the present paper is: (i) Pseudo-boiling is assumed to have liquid-like fluid and gas-like fluid structure. (ii) Physical parameters are well defined at subcritical pressure. Some parameters such as specific heat are defined for both liquid and vapor. Similarly, definitions of parameters are to be given for pseudo-boiling, including pseudo-boiling temperature, corresponding to saturation temperature at subcritical pressure, and pseudo-boiling enthalpy, corresponding to latent heat of evaporation at subcritical pressure. (iii) The original contribution is to introduce pseudo-boiling to deal with SHT. Under heating condition, fluid temperatures are higher near wall and decrease away from wall. Because vapor-like fluid has much smaller thermal conductivity than liquid-like fluid, the wall attached vapor-like layer thickness dominates heat transfer. Two forces are paid attention. The evaporation induced momentum force has the tendency to adhere and grow the vapor-like layer on wall. This force is caused by mass transfer from liquid-like fluid to vapor-like fluid. On the contrary, the inertia force resulted from bulk flow has the tendency to detach the vapor-like layer from wall. The competition of the two forces yields the K number to reflect the pseudo-boiling mechanism on heat transfer.

2.2. Definitions of pseudo-boiling parameters

When a fluid is beyond the critical point, a Widom line (WL) separates the fluid into a liquid-like region and a gas-like region [29]. Fig. 2a shows the phase diagram of CO_2. Interfaced at pseudo-critical temperature T_{pc} (WL line), fluid densities display two regimes distribution: heavier fluid below T_{pc}, and lighter fluid beyond T_{pc} (see Fig. 2b). The two fluids correspond to liquid and vapor at subcritical pressure, respectively. Thus, T_{pc} is defined as

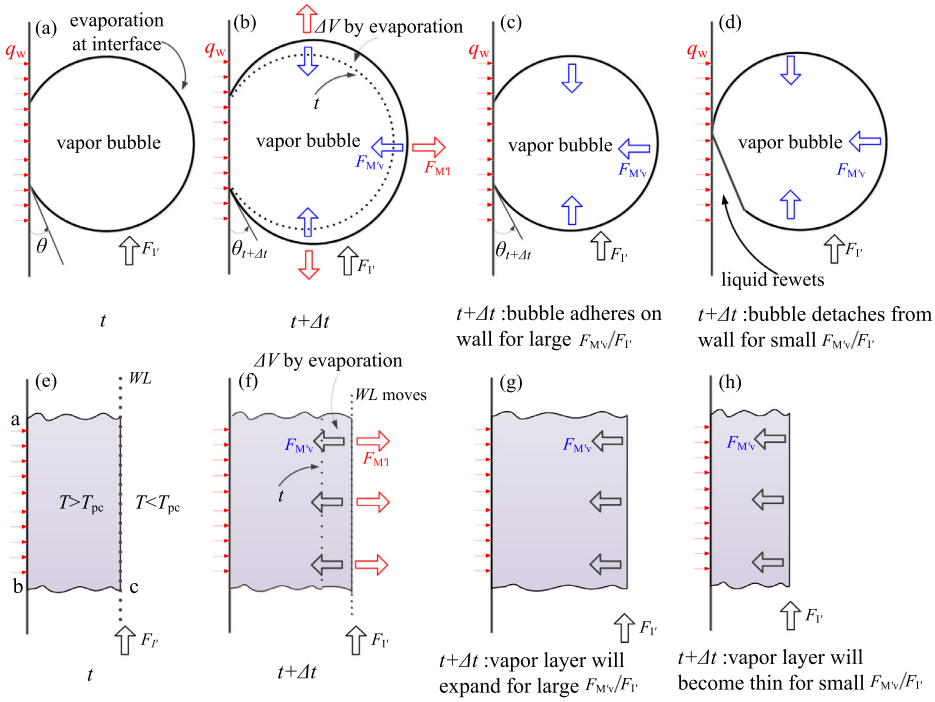

Fig. 3. The physical model showing how the K number representing the competition between evaporation induced momentum force and inertia force dominates if a bubble can detach from wall at subcritical pressure (a-d) and vapor-like fluid layer thickness (e–h) to influence heat transfer, in which ΔV is the volume increase during evaporation, $F_{l'}$ is inertia force, $F_{M'v}$ is evaporation induced momentum force.

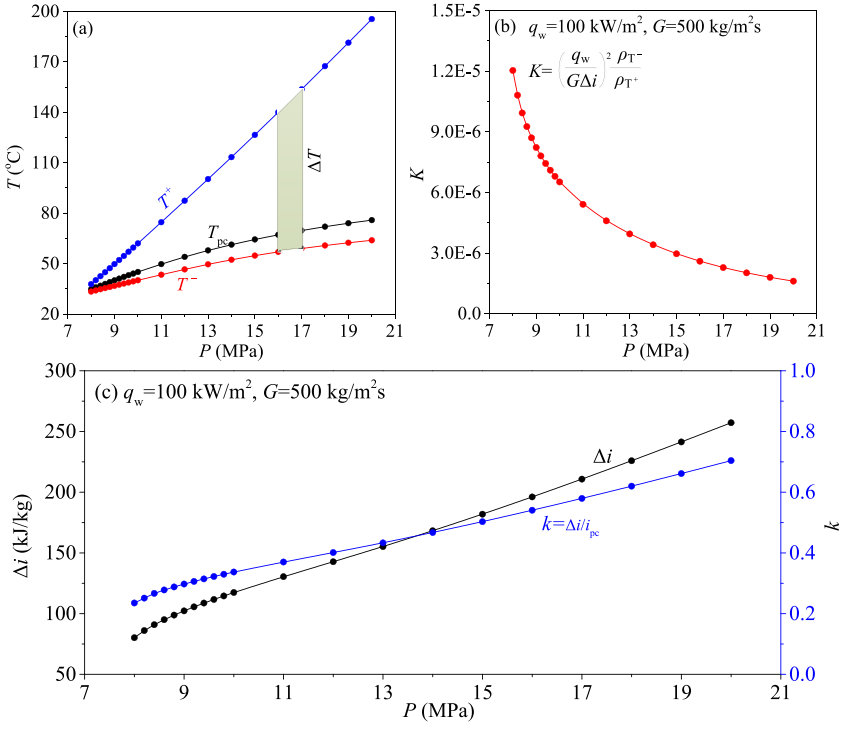

Fig. 4. Effect of pressures on T^-,T^+, Δi and K during pseudo-boiling for S-CO_2

the pseudo-boiling temperature, which is equivalent to saturation temperature in subcritical domain.

Pseudo-boiling enthalpy (Δi) will be defined at supercritical pressure, which is equivalent to latent heat of evaporation (i_{fg}) at subcritical pressure. Fig. 2c shows specific heat to have a peak at T_{pc}. One shall remember that heating to a vapor-liquid system occurs at a saturation temperature in subcritical domain. Latent heat of evaporation quantifies the energy for boiling from liquid to vapor. This situation is changed for supercritical fluid, for which any heating results in a temperature rise. Thus, a temperature T^- be-

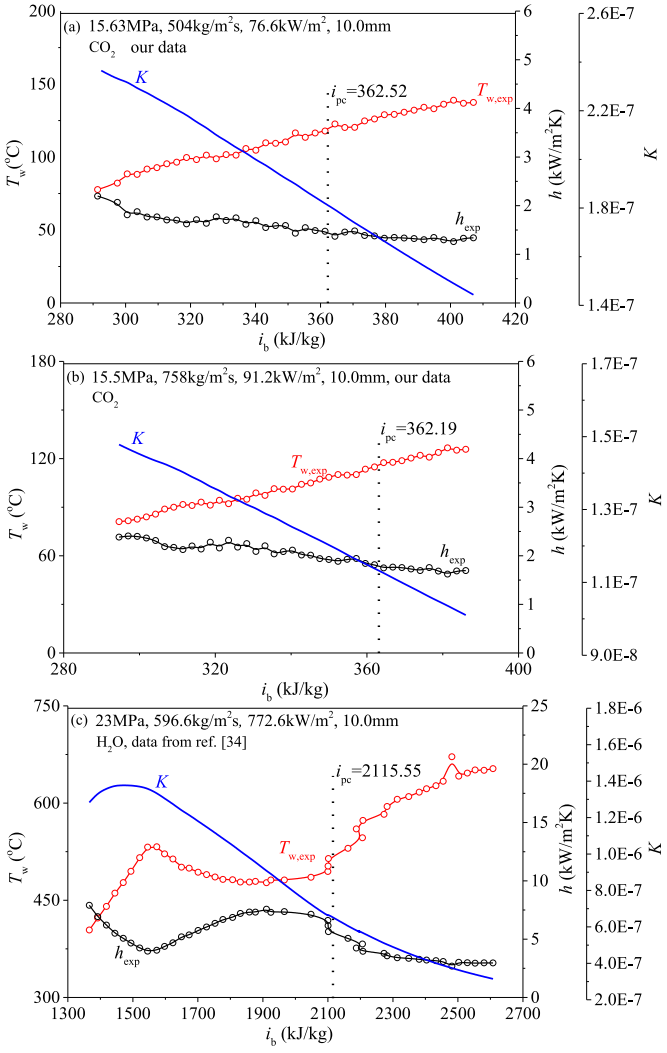

Fig. 5. The K number coincides with the variation trend of inner wall temperatures (a-b for S-CO_2 data, normal heat transfer, c for S-water data, heat transfer deterioration).

low T_{pc} and a temperature T^+ beyond T_{pc} are defined to determine the pseudo-boiling enthalpy (Δi):

$$\Delta i = \int_{T^-}^{T^+} c_p dT = i(T^+) - i(T^-) \tag{1}$$

Physically, Δi overcomes the molecular attraction to widen the molecules distance when crossing the pseudo-critical point. The determination of Δi is seen in Fig. 2c and d. Based on Refs. [30,31], specific heat for liquid-like fluid, $c_{p,l}$, is defined at $\frac{3}{4}T_{pc}$ (see point $\bar{A}$ in Fig. 2c). Specific heat for vapor-like fluid is

$$c_{p,v} = \frac{\gamma R}{\gamma - 1} \tag{2}$$

where γ is the specific heat ratio ($\gamma = 1.15$), R is the gas constant, $R = R_g/M$, R_g is the molar gas constant, which equals to 8.31451 J/mol•K, M is the molar mass of fluid, which equals to 44 g/mol for CO_2.

Fig. 2d shows the enthalpy curve for supercritical fluid over a wide temperature range (black color). Point$\bar{B}$ is marked in the curve at $\frac{3}{4}T_{pc}$ to have an enthalpy of $i_{\bar{B}}$. The curve slope at point $\bar{B}$ equals to $c_{p,l}$, coincided with point $\bar{A}$ in Fig. 2c. Therefore, the enthalpy line for liquid-like fluid, which passes through point $\bar{B}$ and has the slope of $c_{p,l}$, is expressed as

$$i_l = c_{p,l}T + i_{\bar{B}} - \frac{3}{4}c_{p,l}T_{pc} \tag{3}$$

Alternatively, the enthalpy for vapor-like fluid is

$$i_v = c_{p,v}(T + 273.15) \tag{4}$$

We note that the unit of temperature is °C for above deductions. The red curve is the tangent line passing through the pseudo-critical point pc (see Fig. 2d). The tangent line and the i_l line have a crossing point A to determine T^-. The tangent line and the i_v line have a crossing point B to determine T^+. Thus, Δi can be determined with Eq. (1).

2.3. Analogy between subcooled boiling at subcritical pressure and supercritical heat transfer

2.3.1. The K *number for subcooled boiling at subcritical pressure*

Subcooled boiling at subcritical pressure is treated in Fig. 3a–d. A heat flux q_w is applied on a tube wall. A bubble is attached on the wall at time t. Convective flow in the tube imposes an inertia force on the bubble, having the tendency to detach the bubble

Table 2
Experimental database for the present correlation of supercritical heat transfer for vertical up-flow

NO.	Ref. and working fluid	Data range: $P/G/q_w/$	Geometry range: d_{in}/L/Material	Data poins
1	our data CO_2	7.52–20.8 MPa/488–1500 kg•m^{-2}s^{-1}/84–350 kW• m^{-2}	10.0mm/2000mm/1Cr18Ni9Ti	2028
2	[35], CO_2	8.8 MPa/315 kg m^{-2}s^{-1}/31.8–51.95 kW m^{-2}	2.0mm/290mm/1Cr18Ni9Ti	66
3	[36], CO_2	7.75–9.08 MPa/489–874 kg m^{-2}s^{-1}/84.8–216 k m^{-2}	4.5mm/900mm/316L	80
4	[37], CO_2	8.34–8.43 MPa/507–2000 kg m^{-2}s^{-1}/400–350 kW m^{-2}	8.0mm/2000mm/Inconel 600	290
5	[38], CO_2	8.34 MPa/700–2000 kg m^{-2}s^{-1}/40–125 kW m^{-2}	8.0mm/1940mm/ Inconel 600	139
6	[39], CO_2	7.61 MPa/901 kg m^{-2}s^{-1}/175.9–256.2 kW m^{-2}	10.0mm/1200mm/ S32168	40
7	[40], CO_2	8.38–8.8 MPa/784–2000 kg m^{-2}s^{-1}/18.4–161.2 kW m^{-2}	8.0mm/2000mm/not mentioned	44
8	[41], H_2O	23 MPa/596.6 kg m^{-2}s^{-1}/772.6 kW m^{-2}	10.0mm/2500mm/C625	46
9	[42], H_2O	28 MPa/1536 kg m^{-2}s^{-1}/250–585 kW m^{-2}	17.0mm/2000mm/1Cr18Ni9Ti	62
10	[43], H_2O	24–32 MPa/420–800 kg m^{-2}s^{-1}/170–450 kW m^{-2}	19.0mm/2000mm/1Cr18Ni9Ti	356
11	[44], H_2O	23–28 MPa/600 kg m^{-2}s^{-1}/200–300 kW m^{-2}	26.0mm/2000mm/1Cr18Ni9Ti	58
12	[45], H_2O	26–30 MPa/900–1200 kg m^{-2}s^{-1}/300–500 kW m^{-2}	26.0mm/2000mm/1Cr18Ni9Ti	44
13	[46], H_2O	24.1 MPa/499 kg m^{-2}s^{-1}/334 kW m^{-2}	10.0mm/4000mm/ 12Cr18Ni10Ti	62
14	[34], H_2O	23–26 MPa/449–1012 kg m^{-2}s^{-1}/456–696 kW m^{-2}	7.6,10.0mm/2640mm/ Inconel 625	438
15	[47], H_2O	23–26 MPa/450–791.2 kg m^{-2}s^{-1}/450–893.2 kW m^{-2}	10.0mm/2500mm/ Inconel 625	411
16	[48], R134a	4.3 MPa/600–1500 kg m^{-2}s^{-1}/40–50 kW m^{-2}	7.6mm/2300mm/ Inconel 625	218
17	[49], R134a	4.3–4.7 MPa/400-2000 kg m^{-2}s^{-1}/20–140 kW m^{-2}	7.6,10mm/2300mm/ Inconel 625	968
18	[50], R134a	4.3–4.5 MPa/500-1000 kg m^{-2}s^{-1}/40–80 kW m^{-2}	8.0mm/2100mm/ 022Cr17Ni12Mo2	118
19	[51], R134a	4.3 MPa/600 kg m^{-2}s^{-1}/20.17 kW m^{-2}	9.4mm/2000mm/ not mentioned	100

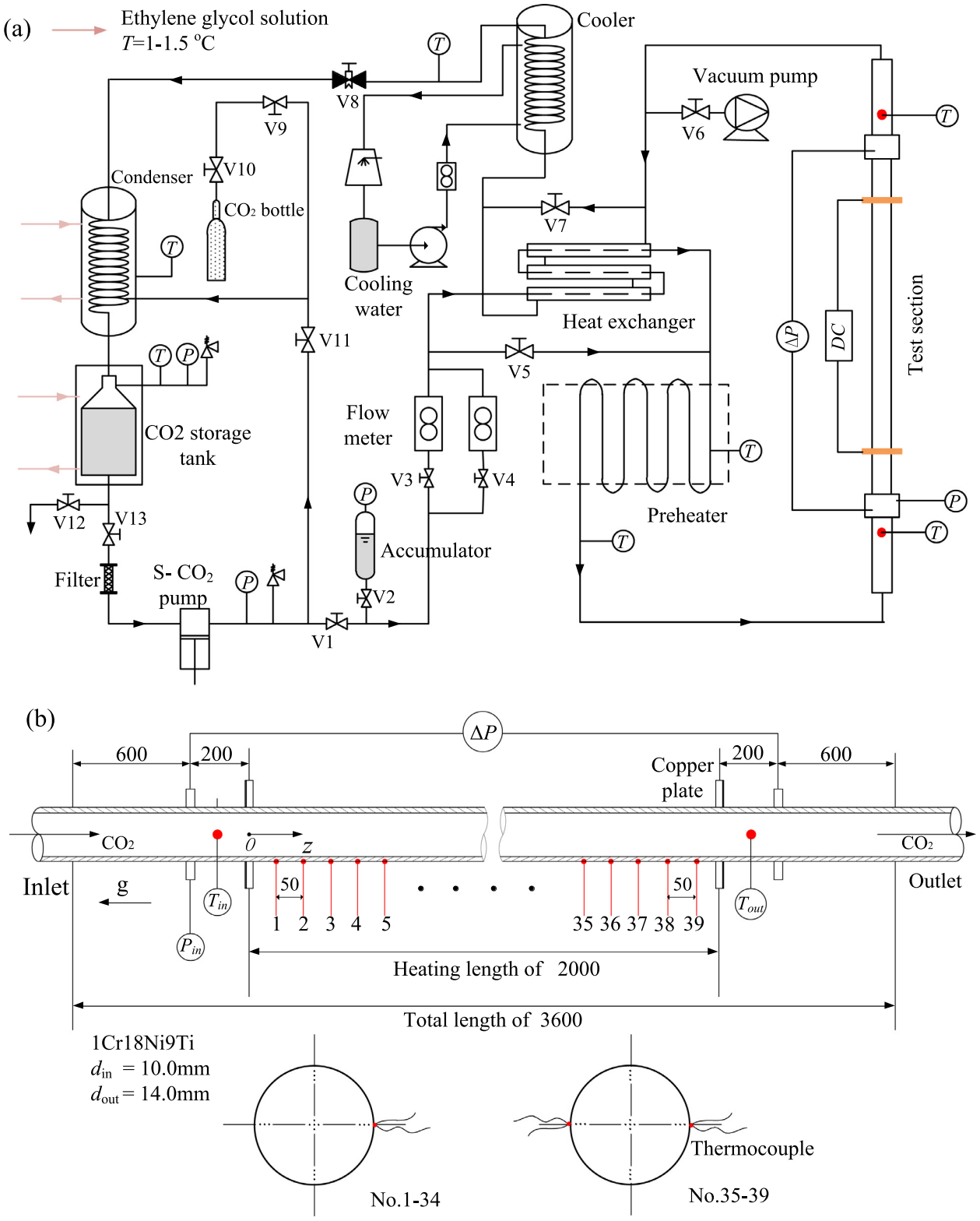

Fig. 6. The experiment setup (a) and the vertically positioned test tube (b).

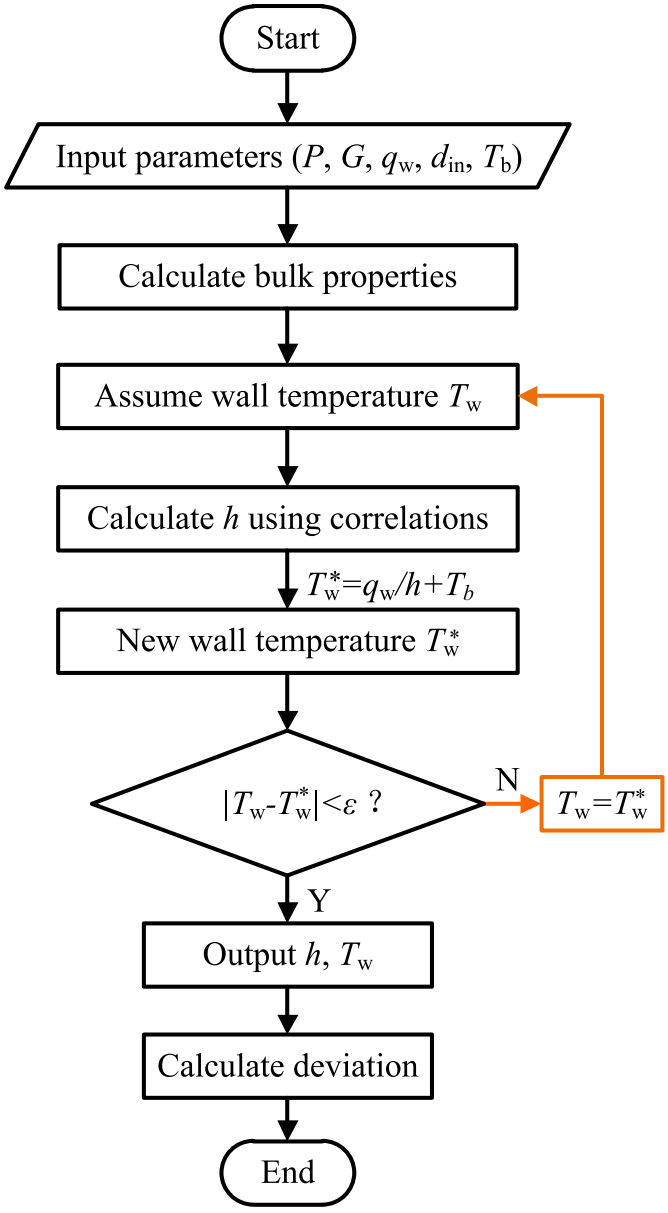

Fig. 7. The determination of h and T_w at given heat flux condition.

from the wall [32].

$$F_{l'} = \frac{G^2 D}{\rho_l} \tag{5}$$

where G is the mass flux, D is the bubble diameter and ρ_l is the liquid density.

From t to $t+\Delta t$, the evaporation at bubble interface induces a mass transfer from liquid to vapor, resulting in an increase of bubble volume of ΔV. Due to bubble expansion, a force $F_{M'l}$ is exerted on the surrounding liquid of bubble. An anti-force $F_{M'v}$ is applied on the bubble, which is called the evaporation induced momentum force [32]:

$$F_{M'v} = \left(\frac{q_w}{i_{fg}}\right)^2 \frac{D}{\rho_v} \tag{6}$$

where i_{fg} is the latent heat of evaporation and ρ_v is the density of vapor. $F_{M'v}$ has the tendency to adhere the bubble on the wall. Therefore, the K number reflects the competition between evaporation induced momentum force and inertia force [32]:

$$K = \frac{F_{M'v}}{F_{l'}} = \left(\frac{q_w}{G \cdot i_{fg}}\right)^2 \frac{\rho_l}{\rho_v} \tag{7}$$

where the term $q_w/(Gi_{fg})$ is the boiling number [32], q_w/i_{fg} scales the mass transfer from liquid to vapor, G represents the inertia effect. A large K number indicates the vapor expansion to attach the bubble on the wall (see Fig. 3c). Coalescence of various bubbles forms a vapor blanket to trigger the wall temperature overshoot, called heat transfer deterioration. Alternatively, a small K number represents large inertia force to detach the bubble from the wall. Thus, the tube wall can be rewetted by liquid to keep better heat transfer performance (see Fig. 3d). The K number has been verified to be useful to characterize the microchannel boiling heat transfer [32,33].

2.3.2. The K number for supercritical heat transfer

Supercritical heat transfer is treated in Fig. 3e–h. Pseudo-boiling assumes a vapor-like fluid near wall and a liquid-like fluid in tube core. The two regions are interfaced at $T = T_{pc}$. Mass transfer on the T_{pc} interface yields the expansion of the vapor-like fluid layer, resulting in evaporation induced momentum force $F_{M'v}$. Replacing i_{fg} in Eq. (7) with Δi in Eq. (1) yields the K number for supercritical heat transfer as

$$K = \left(\frac{q_w}{G \cdot \Delta i}\right)^2 \frac{\rho_{liquid-like}}{\rho_{vapor-like}} \tag{8}$$

where $\rho_{liquid\text{-}like}$ and $\rho_{vapor\text{-}like}$ are the densities of liquid-like fluid and vapor-like fluid. Because the two densities are dependent on temperatures (see Fig. 2b), they are defined at T^- and T^+. Thus, Eq. (8) becomes

$$K = \left(\frac{q_w}{G \cdot \Delta i}\right)^2 \frac{\rho_{T^-}}{\rho_{T^+}} \tag{9}$$

Fig. 4a plots T^+, $T^-$and T_{pc} for S-CO_2. The temperature span ΔT is zero at the critical pressure 7.377 MPa, but increases with increases of pressures. Fig. 4b shows the decreased K number when increasing pressures, indicating the weakened vapor-like fluid layer thickness to improve heat transfer. K also depends on q_w and G, but the change trend is similar to Fig. 4b when q_w and G are changed.

To simplify the calculation of K in Eq. (9), $k = \Delta i/i_{pc}$is introduced. Fig. 4c shows the increased Δi and k versus pressures. Within 8–20 MPa, k covers the range of 0.235-0.704, meaning that Δi and i_{pc} have the same magnitude. In other words, Δi can be scaled as i_{pc}. One notes that the pseudo-boiling theory is in the infancy development stage. The determination of Δi is based on an assumption that the specific heat of liquid $c_{p,l}$ can be defined at $\frac{3}{4}T_{pc}$ [31], which is a rough treatment. Replacing Δi by i_{pc} in Eq. (9) eliminates the uncertainty introduced by the pseudo-boiling enthalpy. Thus, Eq. (9) is modified as

$$K = \left(\frac{q_w}{G \cdot i_{pc}}\right)^2 \frac{\rho_{T^-}}{\rho_{T^+}} \tag{10}$$

The objective of this paper is to develop a general supercritical heat transfer correlation. K in Eq. (10) does not include the information of wall temperatures. Because there is a strong coupling between inner wall temperature T_w, vapor-like layer of supercritical fluid and heat transfer coefficient h, the K number is proposed as

$$K = \left(\frac{q_w}{G \cdot i_w}\right)^2 \frac{\rho_b}{\rho_w} \tag{11}$$

where i_w is the enthalpy at P and T_w, ρ_b and ρ_w are the densities defined at bulk fluid temperature (T_b, heavier fluid) and wall

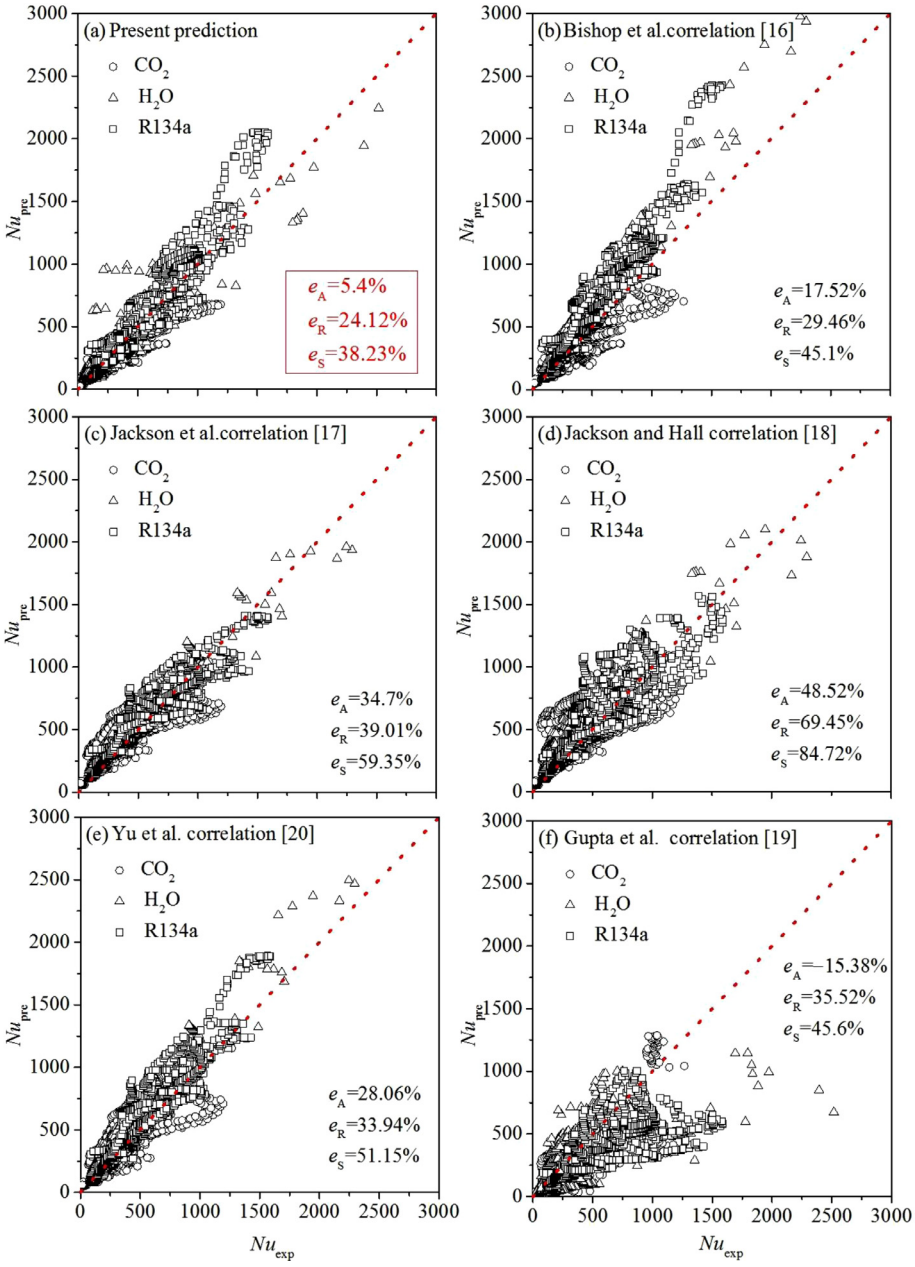

Fig. 8. Comparison of the K number correlation and other correlations with experimental database at given heat fluxes (Nusselt number comparisons).

temperature (T_w, lighter fluid). Physically, the term of $\frac{\rho_b}{\rho_w}$ and the K number defined in Eq. (11) reflect how the relative magnitude of bulk fluid temperature and wall temperature influence the two-phase like structure to affect supercritical heat transfer.

To demonstrate the usefulness of K in Eq. (11), Fig. 5 illustrates the experimentally determined T_w, h and K versus bulk fluid enthalpies i_b along axial flow length. Fig. 5a and b are for our newly obtained CO_2 heat transfer data at $P \approx 16$MPa, while Fig. 5c is for water heat transfer data at P=23 MPa. Supercritical heat transfer can be classified as normal heat transfer such as shown in Fig. 5a and b and heat transfer deterioration with obvious wall temperature peak such as shown in Fig. 5c. Normal heat transfer decreases K number with increases of i_b, but heat transfer deterioration has a peak of K number corresponding to wall temperature overshoot. The variations of K number match the physical meaning regarding its control of the wall-attached vapor-like fluid layer to dominate supercritical heat transfer.

In the literature, supercritical heat transfer is correlated in the framework of single-phase flow (see Table 1). Such treatment is not success when comparing with a large quantity of experiment databases. The contribution of this paper is to introduce the effect of pseudo-boiling induced structure of vapor-like fluid and liquid-like fluid on heat transfer. Among the two-phase like structure, the vapor-like fluid layer dominates heat transfer due to the low thermal conductivity. Because the wall attached vapor-like layer is quantified by the K number, the Nusselt number is correlated in the following form

$$Nu = CRe_b^{n1} Pr_{b,ave}^{n2} K^{n3} \quad (12)$$

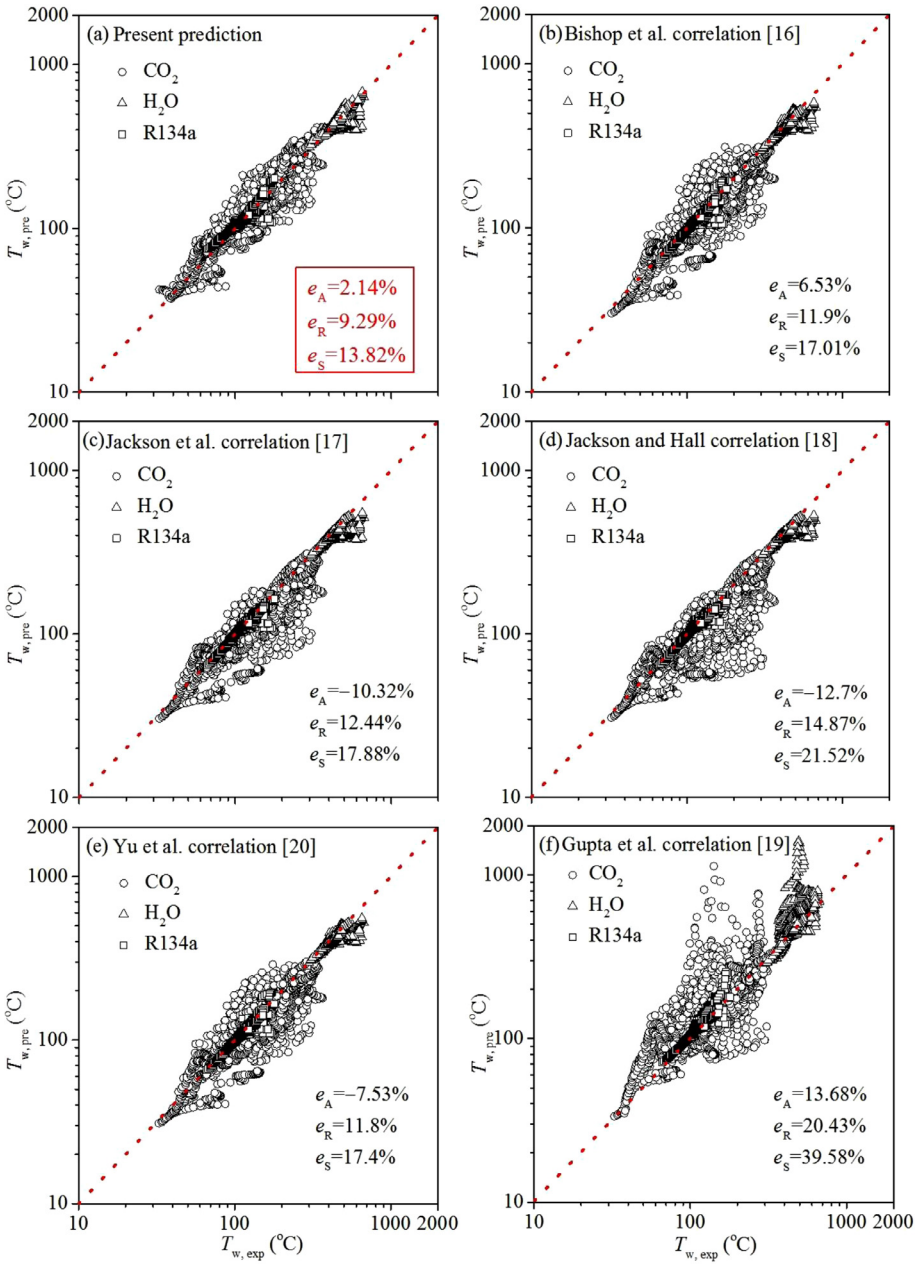

Fig. 9. Comparison of the *K* number correlation and other correlations with experimental database at given heat fluxes (inner wall temperatures comparisons).

where *K* uses Eq. (11), Re_b and $Pr_{b,ave}$ are

$$Re_b = \frac{G \cdot d_{in}}{\mu_b},\ Pr_{b,ave} = \frac{\mu_b \cdot c_{P,ave}}{\lambda_b},\ c_{p,ave} = \frac{i_w - i_b}{T_w - T_b} \tag{13}$$

where d_{in}, i and μ are the inner tube diameter, fluid enthalpy and dynamic viscosity, respectively, the subscripts w and b represent inner wall and bulk fluid conditions, respectively. *Nu* and *h* have the following relationship:

$$Nu_b = \frac{h \cdot d_{in}}{\lambda_b} \tag{14}$$

The coefficients *C* and n1−n3 in Eq. (12) are to be determined by experiment database. In summary, *Re* and *Pr* reflect the convective effect, *K* reflects the effect of pseudo-boiling induced two-phase like structure on heat transfer.

3. Experiment database and *K* number correlation

3.1. Experiment database

To develop a general heat transfer correlation, the following criteria are satisfied: (i) Various working fluids of supercritical water, carbon dioxide and organic fluids are used. (ii) Wide experiment data ranges are covered. The operation pressure of supercritical fluid shall be obviously larger than the critical pressure. Here, the databases of S-CO_2 and water cover the ranges of 8−21 MPa and 23−32 MPa, respectively. The maximum S-CO_2 pressure is up to ~3 times of the critical pressure 7.377 MPa. S-water contains the maximum pressure ~1.5 times of the critical pressure 21.064 MPa. The inner tube diameters cover the range of 2−26 mm. The inner wall heat fluxes cover the range of 18.4−893 kW/m^2. The maxi-

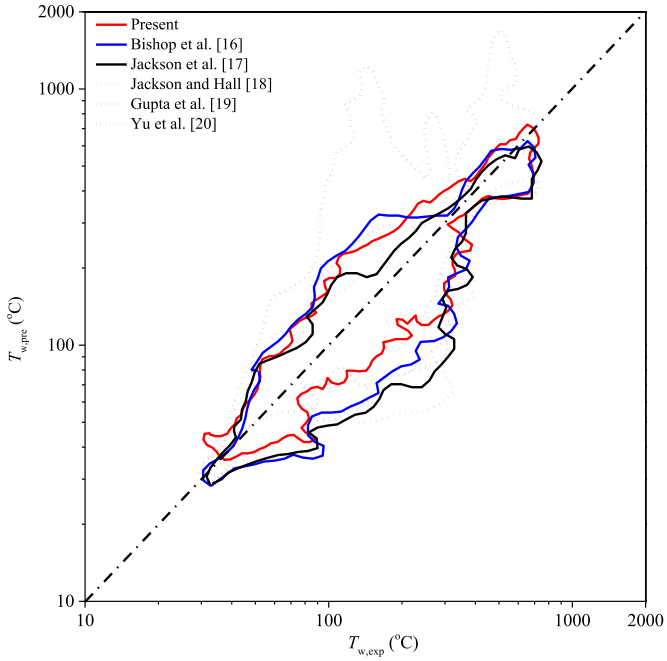

Fig. 10. Envelopes of inner wall temperature predicted by the *K* number correlation and other correlations.

mum heat flux is extremely high for applications. (iii) The database contains not only normal heat transfer data, but also heat transfer deterioration data.

The database is shown in Table 2. Our experiment contributes 2028 data points of S-CO_2. Other 3532 data points are cited from 18 articles for S-CO_2, water and R134a, coming from independent research groups. The parameter ranges are as follows: (i) pressures 4.3−32 MPa; (ii) heat fluxes 20−893 kW/m^2; (iii) mass fluxes 315−2000 kg/m^{2}s; (iv) inner tube diameters 2−26 mm. Various tube lengths L are used in the literature. Almost all of the test tubes have significant large L/d_{in}. Thus, the flow is fully developed to neglect the entrance effect. Different tube materials are applied in experiments, but the material information does not influence the development of heat transfer correlation. The added heat to test tube is used to quantify the inner wall heat flux. Heat loss to environment is carefully considered with thermal efficiency. The selected database satisfies the criteria of duplication, consistence and reproductivity, which were well documented in Ref. [52].

Currently, S-CO_2 cycle is attractive for power generation driven by nuclear energy, solar energy or fossil energy. However, S-CO_2 heat transfer data are insufficient to support the cycle design and operation. Available experiments were performed near the critical pressure ~8 MPa (see Table 2). We expand S-CO_2 data at high pressures. Fig. 6a shows the experimental setup, including a gas-vacuum/CO_2-charging system, a convective CO_2 loop, a cooling water loop and an electric heating system. To eliminate the effect of

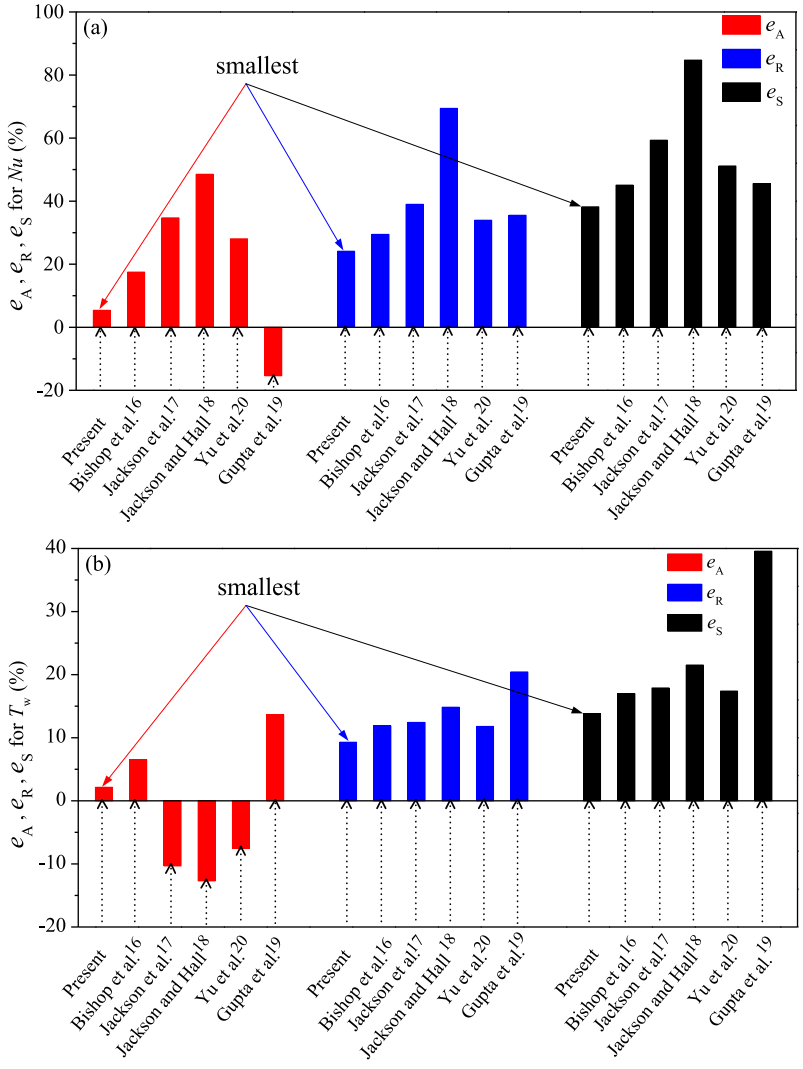

Fig. 11. Summary of the mean error e_A, mean absolute error e_R and square-root error e_S for Nusselt number and inner wall temperatures at given heat fluxes conditions.

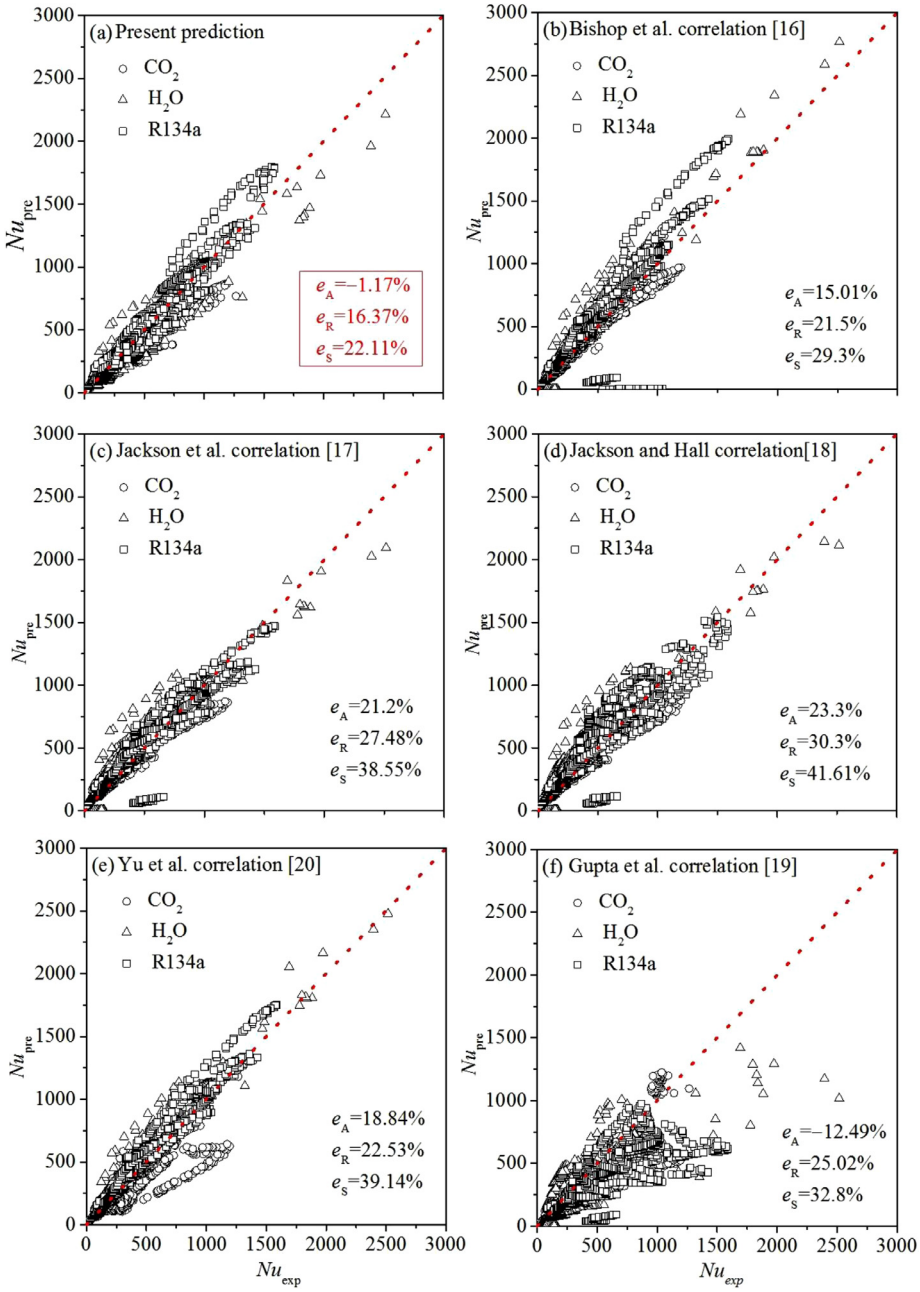

Fig. 12. Comparison of the K number correlation and other correlations with experimental database at given inner wall temperatures.

non-condensable gas on supercritical heat transfer, the system was vacuumed to an ultra-low pressure. The system was then separated from the vacuum pump and charged by CO_2. Here, the 99.99% purity CO_2 was used. Non-condensable gas was further removed by heating the test tube and discharging CO_2 vapor into environment by opening a valve arranged at the highest position of the system. A piston pump circulated CO_2 flow along the loop. The main CO_2 stream flowed through one of the two flow-rate-meters, the tube side of a recuperator heat exchanger, a preheater and a test tube. The CO_2 vapor leaving the test tube entered the shell side of the recuperator heat exchanger and then was cooled by a cooling water loop. The resistance heating principle was used to heat the preheater and the test tube by applying low direct-current (DC) voltage on the tube. The heating power was easily controlled by changing the DC voltage. Thick thermal insulation material was wrapped on the tube to decrease the heat loss to environment.

Fig. 6b shows the test tube made of 1Cr18Ni9Ti, with an outer diameter 14.0 mm and an inner diameter 10.0 mm. The total length was 3600 mm with an effective heating length 2000 mm. To eliminate the thermal resistance between thermocouples and tube wall, thermocouple wires were directly welded on the outer tube surface. Totally, thermocouple wires were arranged on 39 cross-sections, with a neighboring distance of 50 mm. Mass flow rate m was measured either by a DMF-1-3-B Coriolis mass-flow-meter with a range of 0–1000 kg/h, or by a DMF-1-2-A mass-flow-meter with a range of 0–200 kg/h. Both had an uncertainty of 0.2%. The CO_2 pressure at the test tube inlet was measured by a Rosemount 3051 pressure transducer with an uncertainty of 0.1%. Fluid temperatures at the test tube inlet T_{in} and outlet

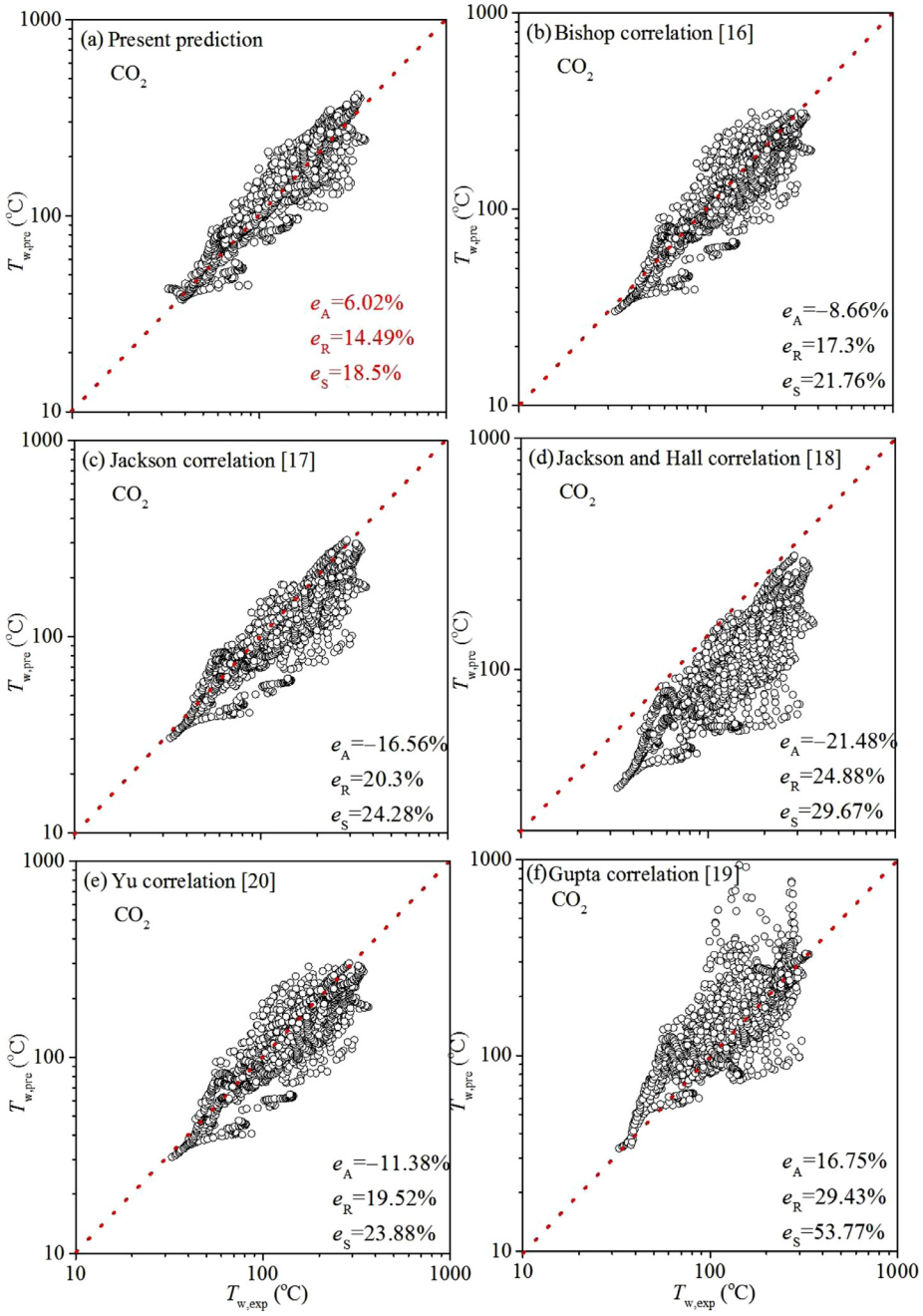

Fig. 13. Comparison of the *K* number correlation and other correlations with CO_2 experimental database at given heat fluxes (inner wall temperatures comparisons).

T_{out} were measured by two jacket thermocouples with an uncertainty of 0.5 °C after calibration. Wall temperature measurements involved an uncertainty of 0.5 °C. A data acquisition system ADAM-4118/4117 collected all the data samples during system operation.

Thermal efficiency η is the CO_2 received heat divided by the resistance heating power measured by a power meter. In our data range, η was ~90%. To eliminate the uncertainty introduced by the power meter, the heating power was determined by $Q = m(i_{out} - i_{in})$. The inner wall heat flux is

$$q_w = \frac{Q}{\pi d_{in} L} = \frac{m(i_{out} - i_{in})}{\pi d_{in} L} \tag{15}$$

where L=2.0 m here. Mass flux is

$$G = \frac{4m}{\pi d_{in}^2} \tag{16}$$

Heat transfer coefficients h are obtained along the axial flow length:

$$h = \frac{q_w}{T_w - T_b} \tag{17}$$

T_w is calculated from the outer wall temperature measurement by using one-dimensional thermal conduction equation [42]. The error transmission principle evaluates the errors of various pa-

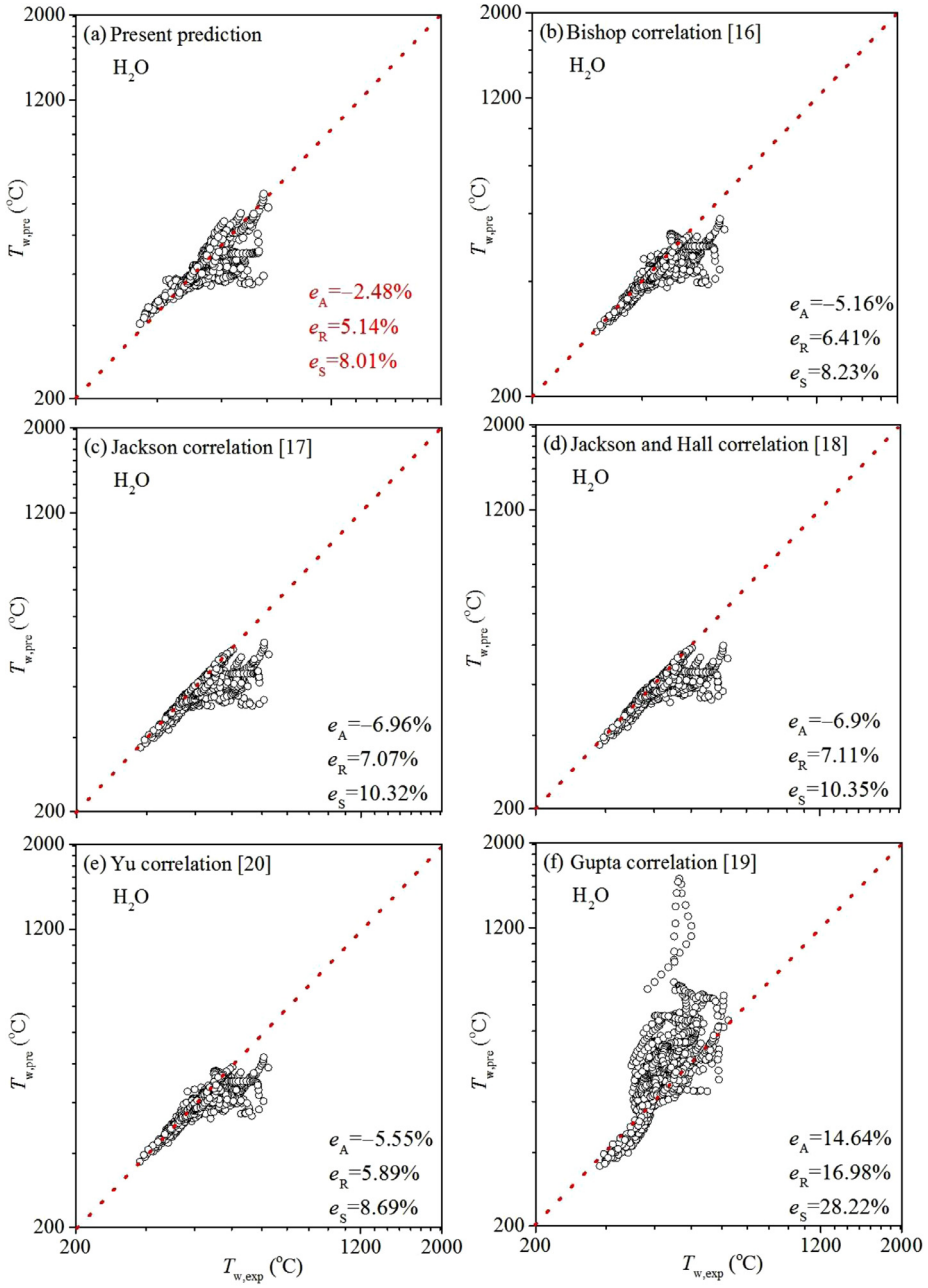

Fig. 14. Comparison of the *K* number correlation and other correlations with H_2O experimental database at given heat fluxes (inner wall temperatures comparisons).

rameters, yielding the uncertainties of 5.05% for q_w and 8.66% for *h*.

3.2. Outcome of the K number correlation

To develop the *K* number correlation, steady-state experiments were selected for our own experiment and other experiments. An experiment run specifies a pressure *P*, a mass flux *G* and an inner wall heat flux q_w. Pressure drop across test tube has neglectable effect on heat transfer. The measured outer wall temperature $T_{w,o}$ is converted to inner wall temperature T_w. Various cross-sections were arranged along axial flow length, each having a T_w and a T_b. The bulk fluid enthalpy i_b is determined by the heat absorption of fluid from the tube inlet to the interest cross-section. On each axial location, *h* and *Nu* are determined using Eqs. (17) and (14), respectively. Eqs. (11) and (13) yield the experimentally determined *K* number, Re_b and $Pr_{b,\,ave}$. The databases shown in Table 2 including S-CO_2, water and R134a help us to develop the *K* number correlation. The task is to achieve *C* and n1–n3 in Eq. (12). Rewriting Eq. (12) yields

$$\ln Nu = \ln C + \mathrm{n1}\cdot \ln Re_b + \mathrm{n2}\cdot \ln Pr_{b,ave} + \mathrm{n3}\cdot \ln K \tag{18}$$

Eq. (18) is expressed as the matrix form$C = (X^TX)^{-1}X^TY$, where *X*, *Y* and *C* are as follows

$$X = \begin{bmatrix} 1\ \ln Re_{b,1}\ \ln Pr_{b,ave,1} \ldots \ln K_1 \\ 1\ \ln Re_{b,2}\ \ln Pr_{b,ave,2} \ldots \ln K_2 \\ \ldots. \\ 1\ \ln Re_{b,n}\ \ln Pr_{b,ave,n} \ldots \ln K_n \end{bmatrix}_{n\times 4},\ Y = \begin{bmatrix} \ln Nu_1 \\ \ln Nu_2 \\ \ldots\ldots \\ \ln Nu_n \end{bmatrix}_{n\times 1},\ C = \begin{bmatrix} \ln C \\ n1 \\ n2 \\ n3 \end{bmatrix}_{4\times 1} \tag{19}$$

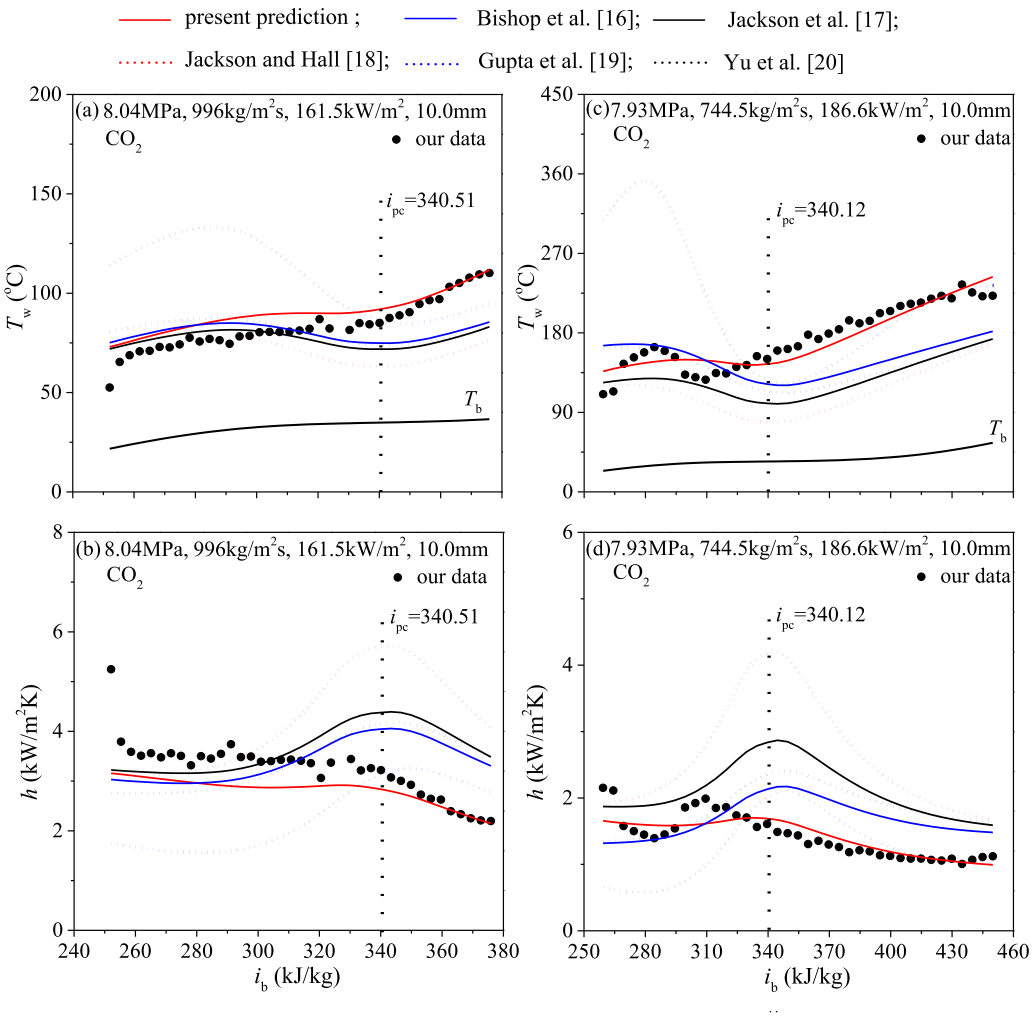

Fig. 15. Assessment of the *K* number correlation and other correlations for S-CO_2 data near the critical pressure.

where n is the total number of data points, which is 5560 in this paper. The K number correlation is

$$Nu = 0.0012 Re_b^{0.9484} Pr_{b,ave}^{0.718} K^{-0.0313} \quad (20)$$

At given P, G, q_w, d_{in} and T_b, Fig. 7 shows the calculation process to determine Nu and T_w. Re_b is directly calculated at given T_b, but $Pr_{b,ave}$ and K are dependent on both T_b and T_w. Initially, a T_w is assumed to decide Nu and h. Thus, a new T_w is determined. The iteration is stopped when satisfying $|T_w - T_w^*| < \varepsilon$, where ε is set as 0.01 K. The calculation process is stopped after several turns of iterations. Eq. (20) using one additional K number correction term only ensures fast iteration and avoids multi-solutions.

4. Results and discussion

It is necessary to perform a thorough comparison between predictions using the K number correlation and experiments. The mean relative error (e_A), mean absolute relative error (e_R) and root-mean-square relative error (e_S) characterize the assessment of predictions using the K number correlation and other correlations in the literature. For a general parameter R, the error for a single data point is

$$e_i = \frac{R_{pre} - R_{exp}}{R_{exp}} \quad (21)$$

where R_{pre} and R_{exp} are the predicted value and measured value, respectively. The three deviation parameters are

$$e_A = \frac{1}{n}\sum_{i=1}^{n} e_i \times 100\%,\ e_R = \frac{1}{n}\sum_{i=1}^{n} |e_i| \times 100\%,\ e_S = \sqrt{\frac{1}{n}\sum_{i=1}^{n} e_i^2} \times 100\% \quad (22)$$

The mean relative error e_A summarizes the overall tendency of the correlation to over-predict or under-predict the measured values. Because e_A concerns the sign of the relative error, positive and negative deviations can offset each other, thus e_A can indicate the error distribution. A small e_A is expected in design stage. The mean absolute relative error e_R describes the arithmetic mean of the absolute errors, expressing correlation accuracy. Alternatively, the root-mean-square relative error emphasizes larger deviations. In following sections, we present a general comparison of our K number correlation and other correlations in the literature with experiment database. Then, we present detailed comparison regarding specific working fluid and operation parameters. Finally, we comment on the K number correlation and future works to be done.

4.1. General assessment of the K number correlation

Recent review articles [9,21,22] show that there are several tens of supercritical heat transfer correlations. Most of these correla-

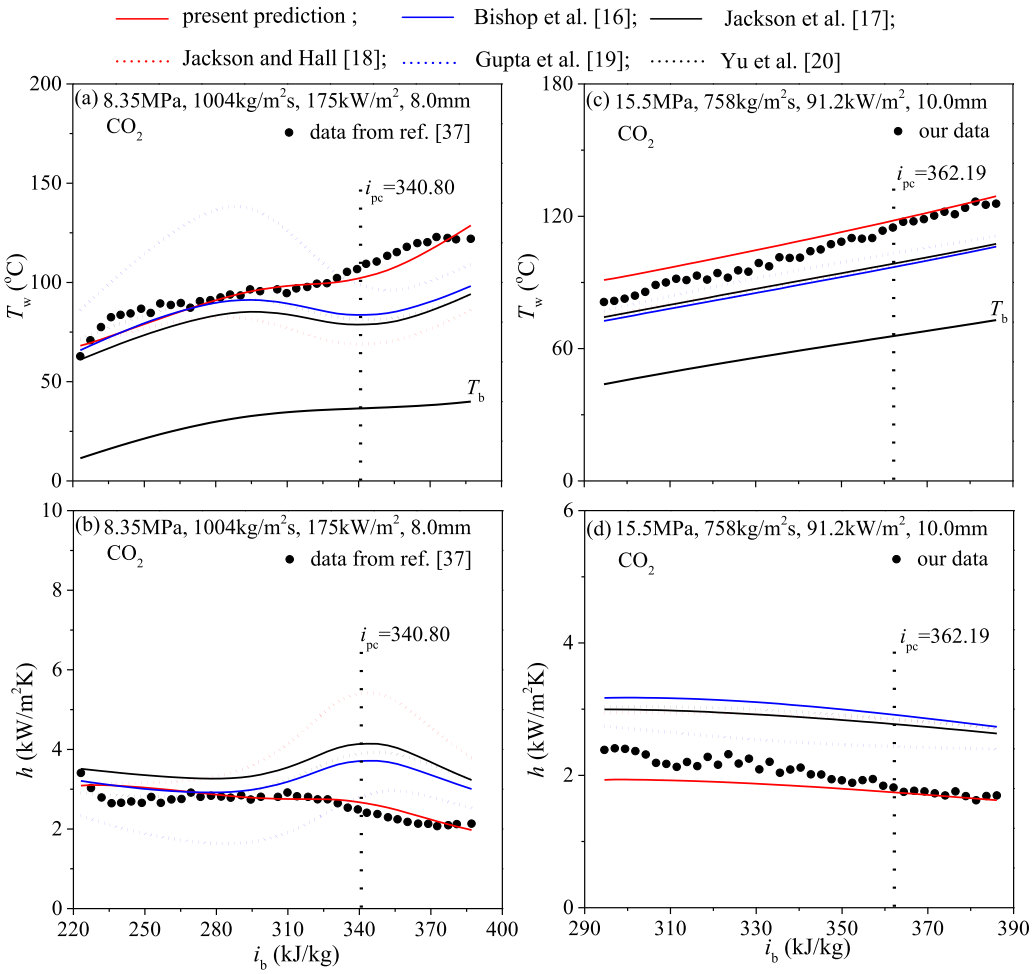

Fig. 16. Assessment of the *K* number correlation and other correlations for S-CO_2 data near the critical pressure and higher pressure.

tions are suitable for narrow data ranges and have poor prediction accuracies when comparing with experiment data. It is difficult to compare the accuracies for all the correlations. It is believed that the five correlations shown in Table 1 have relatively better accuracies than others and they are widely cited in the literature [21,53]. Thus, they are selected in this paper for comparison. Fig. 8 shows the comparison of the *K* number correlation and other correlations with experimentally determined Nusselt number at given heat flux condition. The comparison is performed for 5360 data points with working fluids of CO_2, water and R134a. Our *K* number correlation gives a very small e_A=5.4%, indicating a quasi-symmetry error distribution due to the offsetting effect. The Gupta et al. correlation [19] yields a negative e_A=−15.38%, indicating a larger tendency to under-predict the Nusselt number. The correlations of Bishop et al. [16], Jackson [17], Jackson and Hall [18] and Yu et al. [20] give e_A values of 17.52%, 34.7%, 48.52% and 28.06%, respectively, severely over-estimating the Nusselt number. Our *K* number correlation gives the mean absolute relative error (e_R) of 24.12%, which is acceptable for applications. The other five correlations give e_R larger than 30%, for example, the Jackson & Hall correlation [18] gives e_R up to 69.45%, failing to predict the Nusselt number. We note that e_S apparently amplifies relative error, which is e_S=38.23% for our *K* number correlation. This value is the smallest by comparing with other correlations. In summary, our *K* number correlation gives the best estimation, while the Bishop et al. correlation [16] is the secondary better one for *Nu* estimation.

One is more interest to inner wall temperatures T_w from application point of view. T_w covers a wide range, inspiring us to use logarithm coordinates in Fig. 9. Generally, e_A, e_R and e_S for T_w are smaller than those for *Nu*. Our *K* number correlation yields e_A=2.14%, e_R=9.29% and e_S=13.82%, which are sufficiently accurate to estimate heater surface temperatures. The signs of e_A in Fig. 9c–f for T_w are inverse to those in Fig. 8c–f for *Nu*. The correlations of Jackson [17], Jackson and Hall [18] and Yu et al. [20] have the tendency to under-predict T_w, which are not safe for applications. The Gupta et al. [19] correlation has the tendency to over-predict T_w.

To further identify the deviations between predictions and experiment data, Fig. 10 shows the envelopes of inner wall temperatures. The present correlation gives the smallest envelope against the line of $T_{w,pre}$=$T_{w,exp}$. Fig. 11 summarizes the error indexes among the six correlations. In summary, Figs. 8–9 identify much better prediction accuracy of the *K* number correlation than other correlations at given heat flux condition. Eq. (20) is also convenient to calculate Nusselt number and heat transfer coefficient when inner wall temperature is known, called the given wall temperature condition. Under such circumstance, it is not necessary to iterate the calculation. Fig. 12 shows the comparison outcome, having similar conclusion to the given heat flux condition. The Gupta et al. correlation [19] presents very scattered error distribution.

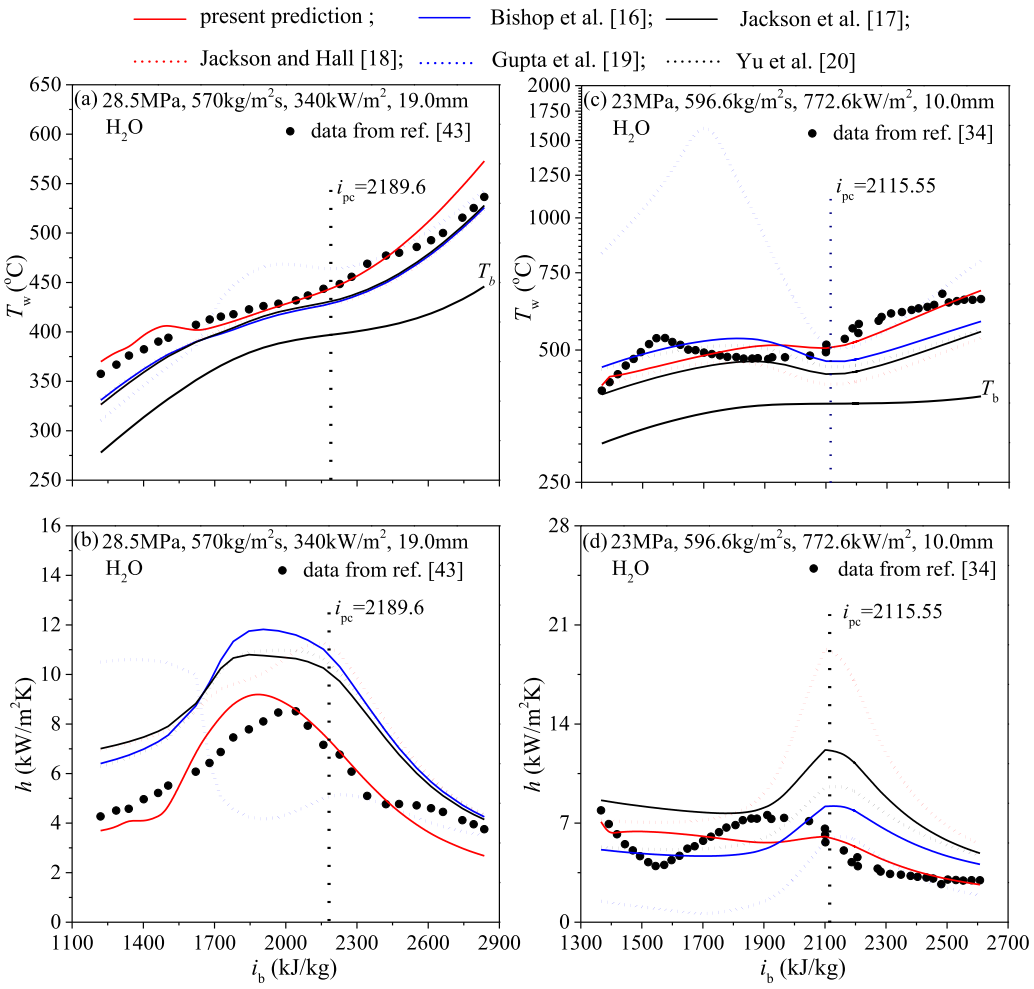

Fig. 17. Assessment of the *K* number correlation and other correlations for S-water data. (For interpretation of the references to color in this figure, the reader is referred to the web version of this article.)

4.2. Comparison with experiments for specific working fluid

In order to select suitable correlation for specific fluid, comparisons were presented in Fig. 13 for CO_2 and Fig. 14 for water. The general conclusion is similar to those shown in Figs. 8–12. The *K* number correlation gives the best estimation among the six correlations, while the Bishop et al. correlation [16] is the secondary better one. The five correlations in Table 1 are observed to give poorer accuracies for CO_2 than those for water. Supercritical heat transfer of CO_2 is a new topic that is being addressed in this stage.

The general applicability of the *K* number correlation is verified by comparing predictions with experiment data for three working fluids and different pressures, heat fluxes, mass fluxes and tube diameters. Figs. 15–18 demonstrate detailed comparison regarding wall temperatures T_w and heat transfer coefficients h versus bulk fluid enthalpies i_b. Figs. 15 and 16 are for CO_2 data near the critical pressure ~8 MPa and higher pressure 15.5 MPa. Fig. 17 is for water data at 28.5 MPa and 23 MPa, and Fig. 18 is for R134a data at 4.5 MPa and 4.3 MPa. It is seen that the solid-red curves of the *K* number correlation gave perfect agreement with the experiment determined T_w and h, not only in the region with enthalpies smaller than i_{pc}, but also in the region with enthalpies larger than i_{pc}. This is because the *K* number correlation successfully treats the pseudo-boiling phenomenon.

The prediction capabilities of other correlations are discussed. For most of runs, predictions by the Gupta et al. correlation [19] intersect the experiment data. The correlation severely over-predicts T_w in $i<i_{pc}$ region, crosses with T_w near the pseudo-critical point, and then under-predicts T_w in $i>i_{pc}$ region (see Figs. 15–18). Correspondingly, the correlation significantly over-estimates heat transfer coefficients beyond the pseudo-critical point. The correlations of Bishop et al. [16], Jackson [17], Jackson and Hall [18] and Yu et al. [20] give acceptable accuracies in low enthalpy region with $i<i_{pc}$. However, beyond the pseudo-critical point, they apparently under-predict T_w and over-predict h. The Jackson & Hall correlation [18] gives the poorest accuracies.

In this paper, heat transfer coefficient is a function of *Re*, *Pr* and *K*, in which *K* scales the vapor-like fluid layer thickness. The better prediction accuracy comes from the success treatment of the pseudo-boiling induced fluid structure. Fig. 19 further identifies the connection between *K* and h. At same G, q_w and d_{in} for CO_2, our experiments show that by raising pressures from 8.22 MPa to 20.80 MPa, heat transfer coefficients are obviously increased. Correspondingly, *K* is smaller at higher pressures. Our correlation outcome gives a negative exponent −0.0313 for *K* indicates the improved heat transfer by raising pressures, agreeing with the observed heat transfer behavior. Fig. 19 demonstrates the logic that a larger *K* corresponds to a larger evap-

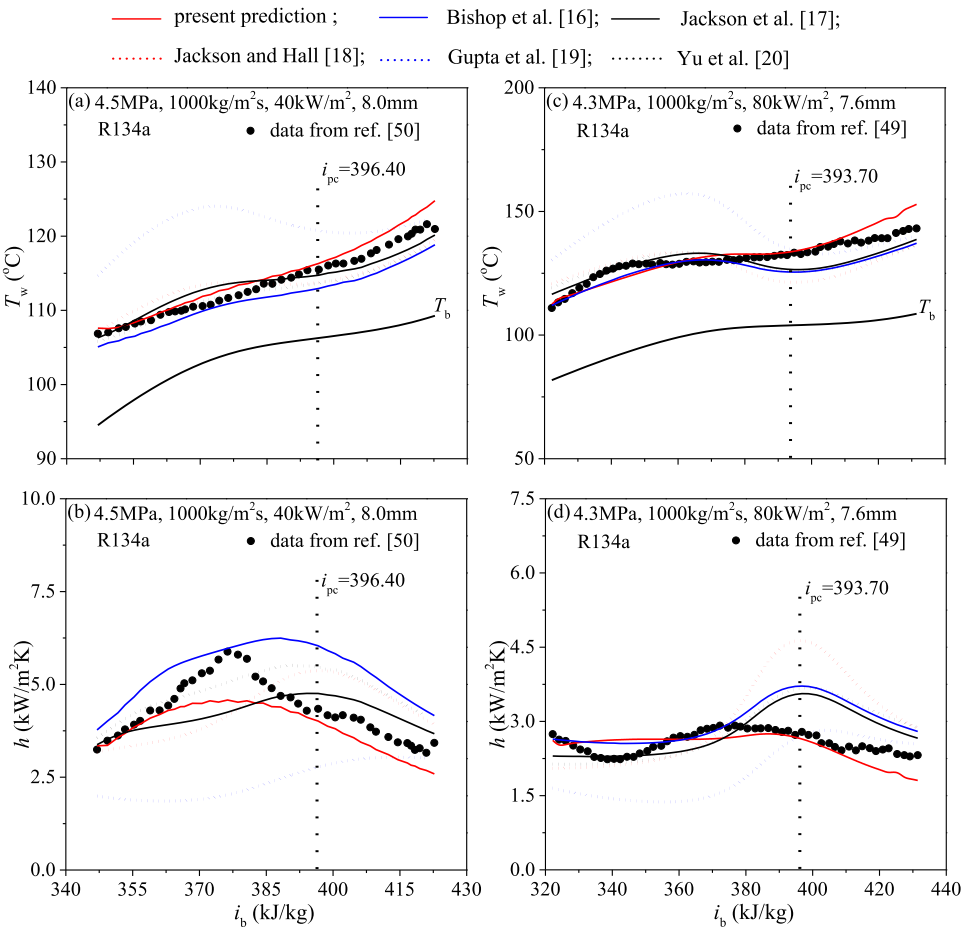

Fig. 18. Assessment of the K number correlation and other correlations for S-R134a data.

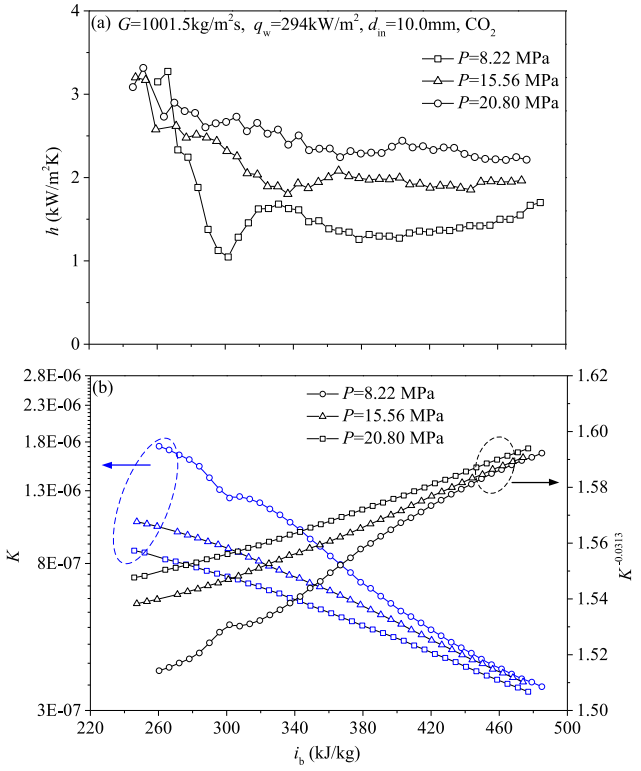

Fig. 19. Relationship between h and K to demonstrate correctly physical meaning of $K^{-0.0313}$ by varying pressures.

oration induced momentum force competed with inertia force, increasing the vapor-like fluid layer thickness to weaken heat transfer.

4.3. Comparison with experiments beyond the database for the K number correlation

One notes that the K number correlation is based on the database including 5560 data points. To demonstrate the general prediction capability of the K number correlation, Figs. 20 and 21 further show comparisons with experiment data. Even though CO_2, water and R134a are still used in Fig. 20, the experiment data cited from Refs [54–56] are not included in the database. Perfect agreement between predictions and experiments is observed, except the slight deviation for water shown in Fig. 20b. Fig. 21 shows the general prediction capability of the K number correlation by randomly selecting a working fluid R22, whose heat transfer data come from Refs. [57,58]. Our correlation excellently matches the experimentally determined wall temperatures, with the deviation of 1–4 K covering whole flow length.

The reason why other correlations in the literature gave poorer accuracies is discussed. The correlations of Bishop et al. [16], Jackson [17] and Jackson and Hall [18] used the correction terms of density and specific heat defined at wall temperature with respect to bulk fluid temperature, which are classical treatment of convective heat transfer, not reflecting “boiling” when approaching or beyond the pseudo-critical point. Introducing one more correction term of viscosity even yields poorer prediction results, see predictions by the Gupta et al. correlation [19] in Figs. 12–15. The

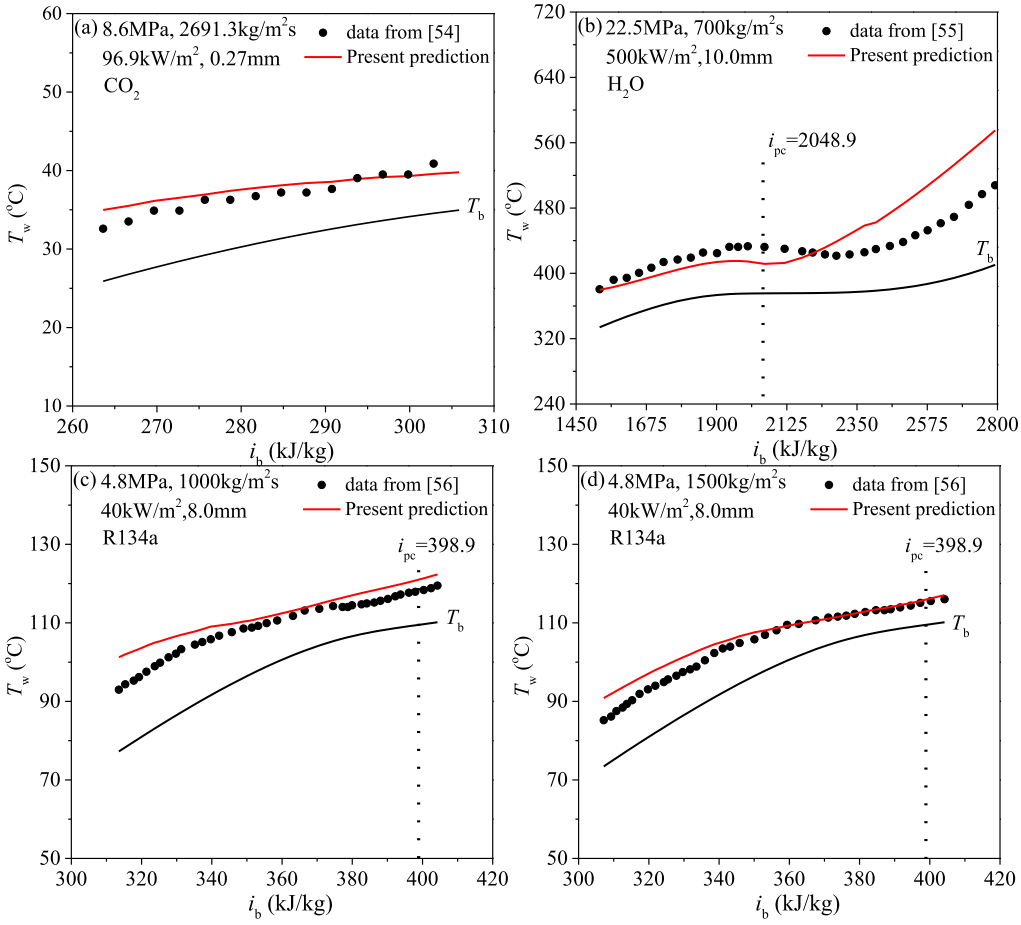

Fig. 20. Comparisons between predictions by the *K* number correlation and experiments beyond the experimental database for the *K* number correlation.

Yu et al. [20] correlation introduced buoyancy effect and acceleration effect, but the situation is not improved too much. In summary, the assumption of single-phase, homogeneous structure accounts for poor prediction accuracies with available heat transfer correlations. This work demonstrates that indeed, it is necessary to consider the pseudo-boiling when dealing with supercritical heat transfer.

Supercritical heat transfer can be classified as normal heat transfer and heat transfer deterioration. The widely accepted criteria to judge HTD do not exist in the literature. Refs. [59–61] proposed the following criteria

$$h/h_{D-B} < 0.3 \text{ or } 0.5 \tag{23}$$

where h is the practical heat transfer coefficient, $h_{D\text{-}B}$ is the Dittus–Boelter heat transfer coefficient:

$$h_{D-B} = \frac{\lambda_b}{d_{in}} \cdot 0.023 Re_b^{0.8} Pr_b^{0.4} \tag{24}$$

Eq. (23) is questioned by other researchers [62]. This is because sometimes, normal heat transfer case also satisfies Eq. (23). Zhu et al. [63] proposed the criterion $\frac{q_W}{G \cdot i_{pc}} > 5.126 \times 10^{-4}$ for CO_2 in vertical up-flow tubes, which is a reliable criterion to judge the onset of HTD. For supercritical heat transfer of water, even though many studies have been performed and several criteria for heat transfer deterioration exist in the literature, these criteria have poor prediction accuracies [13,62]. Because the *K* number correlation makes a strong link between wall temperature, "boiling" structure and heat transfer, the correlation captures reasonable wall temperatures for SHT.

Future works are suggested as follows: (i) The heterogeneous structure of supercritical fluid is to be explored from microscopic point of view. (ii) Numerical/theoretical works are suggested to incorporate pseudo-boiling. (iii) Supercritical heat transfer correlations are to be established for non-circular channels, different channel inclination angles and non-uniform heating boundary conditions. (iv) The mechanism and correlation for heat transfer deterioration are to be developed incorporating the pseudo-boiling mechanism.

5. Conclusions

Following conclusions can be drawn:

- Pseudo-boiling occurs within a temperature span, which is defined here. Pseudo-boiling enthalpy is increased with pressures, which can be scaled as the enthalpy at pseudo-critical temperature.
- The *K* number for supercritical heat transfer (SHT) is proposed to reflect vapor-like fluid layer expansion induced momentum force competed with inertia force. SHT is correlated with only one correction term of the *K* number except *Re* and *Pr*, ensuring fast convergence and avoiding multi-solutions.
- Expanded experiment database for S-CO_2 heat transfer is performed with pressures up ~3 times of the critical pressure. The present experiments along with other experiments in the literature including 5560 data points for CO_2, water, R134a are used to achieve the coefficient and exponents in the *K* number correlation.

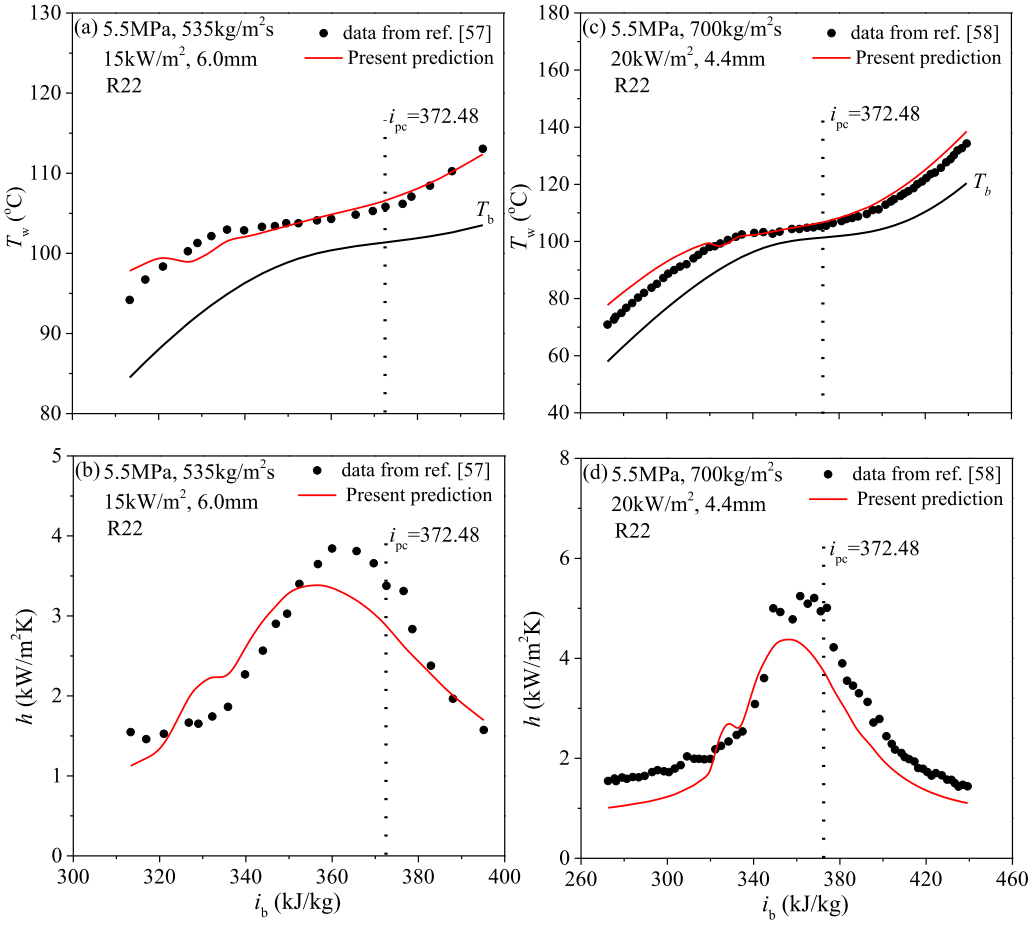

Fig. 21. Comparisons between predictions by the *K* number correlation and experiments for a randomly selected working fluid of R22.

- Covering entire fluid enthalpy region, the *K* number correlation has acceptable prediction accuracy, which is the best among the six heat transfer correlations. Other correlations in the literature have large deviations from experiments when approaching or beyond the pseudo-critical point.
- The general predication capability of the *K* number correlation is verified by comparing with experiments of randomly selected working fluid not included in the database for the development of the *K* number correlation.
- Future works regarding pseudo-boiling and heterogeneous structure of supercritical fluids are recommended.

Author statement

We state that the paper titled as " The general supercritical heat transfer correlation for vertical up-flow tubes: *K* number correlation " by Bingguo Zhu, Jinliang Xu, Chenshuai Yan, Jian Xie to Int J Heat and Mass Transfer, has not been published previously and will not be submitted to elsewhere before we receive your decision.

Declaration of Competing Interest

The authors declared that there is no conflict of interest.

Acknowledgements

The study was supported by the National Key R&D Program of China (2017YFB0601801), the National Natural Science Foundation of China (51821004), the Fundamental Research Funds for the Central Universities (2018ZD02).

References

[1] W.C. Tsai, Y. Wang, Progress of supercritical fluid technology in polymerization and its applications in biomedical engineering, Prog. Polym. Sci. 98 (2019) 101161.
[2] Z. Knez, E. Markocic, M. Leitgeb, M. Primozic, M. Knez, M. Skerget, Industrial applications of supercritical fluids: a review, Energy 77 (2014) 235–243.
[3] J. Xu, E. Sun, M. Li, H. Liu, B. Zhu, Key issues and solution strategies for supercritical carbon dioxide coal fired power plant, Energy 157 (2018) 227–246.
[4] G. Tsiklauri, R. Talbert, B. Schmitt, G. Filippov, R. Bogoyavlensky, E. Grishanin, Supercritical steam cycle for nuclear power plant, Nucl. Eng. Des. 235 (2005) 1651–1664.
[5] V. Dostal, A Supercritical Carbon Dioxide Cycle For Next Generation Nuclear Reactors Ph.D. thesis, Massachusetts Institute of Technology, Cambridge, 2004.
[6] K. Wang, M. Li, J. Guo, P. Li, Z. Liu, A systematic comparison of different S-CO_2 Brayton cycle layouts based on multi-objective optimization for applications in solar power tower plants, Appl. Energy 212 (2018) 109–121.
[7] E. Sun, J. Xu, M. Li, G. Liu, B. Zhu, Connected-top-bottom-cycle to cascade utilize flue gas heat for supercritical carbon dioxide coal fired power plant, Energy Convers. Manag. 172 (2018) 138–154.
[8] K. Shahverd, R. Loni, B. Ghobadian, Monem, S. Gohar, S. Marof, G. Najaf, Energy harvesting using solar ORC system and Archimedes Screw Turbine(AST) combination with different refrigerant working fluids, Energy Convers. Manag. 187 (2019) 205–220.
[9] M. Pizzarelli, The status of the research on the heat transfer deterioration in supercritical fluids: a review, Int. Commun. Heat Mass 95 (2018) 132–138.
[10] J. Xu, C. Liu, E. Sun, J. Xie, M. Li, Y. Yong, J. Liu, Perspective of S-CO_2 power cycles, Energy 186 (2019) 115831.
[11] I.L. Pioro, R.B. Duffey, Experimental heat transfer in supercritical water flowing inside channels (survey), Nucl. Eng. Technol. 235 (2005) 2407–2430.
[12] Y.A. Cengel, M.A. Boles, in: Thermodynamics An Engineering Approach, fifth ed., McGraw-Hill, New York, 1991, pp. 117–137.
[13] D. Huang, Z. Wu, B. Sunden, W. Li, A brief review on convection heat transfer of fluids at supercritical pressures in tubes and the recent progress, Appl. Energy 162 (2016) 494–505.

[14] F. Li, B. Bai, A model of heat transfer coefficient for supercritical water considering the effect of heat transfer deterioration, Int. J. Heat Mass Transf. 133 (2019) 316–329.
[15] X. Lei, Y. Guo, W. Zhang, H. Li, L. Li, Development of heat transfer correlation for supercritical water in vertical upward tubes, Heat Transf. Eng. 40 (8) (2019) 652–666.
[16] A.A. Bishop, R.O. Sandberg, L. Tong, in: Forced Convection Heat Transfer to Water at Near-Critical Temperatures and Super-Critical Pressures, Westinghouse Electric Corporation, Atomic Power Division, Pittsburgh, PA, USA, 1964 Report WCAP-2056.
[17] J.D. Jackson, Fluid flow and convective heat transfer to fluids at supercritical pressure, Nucl. Eng. Des. 264 (2013) 24–40.
[18] J.D. Jackson, W.B. Hall, Influences of buoyancy on heat transfer to fluids flowing in vertical tubes under turbulent conditions, turbulent forced convection in channels and bundles, Hemisphere 2 (1979) 613–640.
[19] S. Gupta, E. Saltanov, S.J. Mokry, I.P. Trevani, L.D.M. Gillivray, Developing empirical heat-transfer correlations for supercritical CO_2 flowing in vertical bare tubes, Nucl. Eng. Des. 261 (2013) 116–131.
[20] J. Yu, B. Jia, D. Wu, D. Wang, Optimization of heat transfer coefficient correlation at supercritical pressure using genetic algorithms, Heat Mass Transf. 45 (2009) 757–766.
[21] M.M. Ehsan, Z. Guan, A.Y. Klimenko, A comprehensive review on heat transfer and pressure drop characteristics and correlations with supercritical CO_2 under heating and cooling applications, Renew. Sust. Energy Rev. 92 (2018) 658–675.
[22] H. Wang, L.K.H. Leungc, W. Wang, Q. Bi, A review on recent heat transfer studies to supercritical pressure water in channels, Appl. Therm. Eng. 142 (2018) 573–596.
[23] D. Huang, W. Li, A brief review on the buoyancy criteria for supercritical fluids, Appl. Therm. Eng. 131 (2018) 977–987.
[24] K Nishikawa, K. Miyabe, in: On the Boiling-Like Phenomena at Supercritical Pressures, Memoirs of Faculty of Engineering, 25, Kyushu University, 1965, pp. 1–25.
[25] J.W. Ackerman, Pseudo-boiling heat transfer to supercritical pressure water in smooth and ribbed tubes, J. Heat Trans. (1970) 490–497.
[26] J. Wang, H. Li, S. Yu, T. Chen, Comparison of the heat transfer characteristics of supercritical pressure water to that of subcritical pressure water in vertically-upward tubes, Int. J. Multiph. Flow 37 (2011) 769–776.
[27] J.P. Holman, S.N. Rea, C.E. Howard, Forced convection heat transfer to Freon 12 near the critical state in a vertical annulus, Int. J. Heat Mass Transf. 8 (1965) 1095–1102.
[28] E. Stewart, P. Stewart, A. Watson, Thermo-acoustic oscillations in forced heat transfer to supercritical pressure water, Int. J. Heat Mass Transf. 16 (1973) 257–270.
[29] G.G. Simeoni, T. Bryk, F.A. Gorelli, M. Krisch, G. Ruocco, M. Santoro, et al., The Widom line as the crossover between liquid-like and gas-like behavior in supercritical fluids, Nat. Phys. 6 (2010) 503–507.
[30] D.T. Banuti, Crossing the Widom-line–supercritical pseudo-boiling, J. Supercrit. Fluids 98 (2015) 12–16.
[31] D.T. Banuti, Thermodynamic Analysis and Numerical Modeling of Supercritical Injection, Institute of Aerospace Thermodynamics University of Stuttgart, 2015 Ph.D. thesis.
[32] S.G. Kandlikar, Heat transfer mechanisms during flow boiling in micro channels, J. Heat Transf. 126 (2014) 8–16.
[33] J. Xu, S. Shen, Y. Gan, Y. Li, W Zhang, Q. Su, Transient flow pattern based micro scale boiling heat transfer mechanisms, J. Micromech. Microeng. 15 (2015) 1344–1361.
[34] L. Wang, Research on Heat Transfer Characteristics of Supercritical Water in Vertical Bare Tube (Master Thesis), School of Mechanical Engineering, Shanghai Jiaotong University, 2012.
[35] Z. Li, P. Jiang, C. Zhao, Y. Zhang, Experimental investigation of convection heat transfer of CO_2 at supercritical pressures in a vertical circular tube, Exp. Therm. Fluid Sci. 34 (2010) 1162–1171.
[36] D.E. Kim, M.H. Kim, Experimental investigation of heat transfer in vertical upward and downward supercritical CO_2 flow in a circular tube, Int. J Heat Fluid Flow. 32 (1) (2011) 176–191.
[37] K. Jiang, An Experimental Facility For Studying Heat Transfer in Supercritical Fluids Ph.D. thesis, Ottawa-Carleton Institute for Mechanical and Aerospace Engineering, 2015.
[38] H. Zahlan, D.C. Groeneveld, S. Tavoularis, Measurements of convective heat transfer to vertical upward flows of CO_2 in circular tubes at near-critical and supercritical pressures, Nucl. Eng. Des. 289 (2015) 92–107.
[39] S. Liu, Y. Huang, G. Liu, J. Wang, L.K.H. Leung, Improvement of buoyancy and acceleration parameters for forced and mixed convective heat transfer to supercritical fluids flowing in vertical tubes, Int. J Heat Mass Transf. 106 (2017) 1144–1156.
[40] I. Pioro, S. Gupta, S. Mokry, Heat-transfer correlations for supercritical-water and carbon dioxide flowing upward in vertical bare tubes, in: Proceedings of the ASME 2012 Summer Heat Transfer Conference, Rio Grande, Puerto Rico, 2012 July 8-12.
[41] G. Zhang, H. Zhang, H. Gu, Y. Yang, X. Cheng, Experimental and numerical investigation of turbulent convective heat transfer deterioration of supercritical water in vertical tube, Nucl. Eng. Des. 248 (2012) 226–237.
[42] Z. Shen, D. Yang, G. Chen, F. Xiao, Experimental investigation on heat transfer characteristics of smooth tube with downward flow, Int. J. Heat Mass Transf. 68 (2014) 669–676.
[43] Z. Shen, Yang D, H. Xie, X. Nie, W. Liu, S. Wang, Flow and heat transfer characteristics of high-pressure water flowing in a vertical upward smooth tube at low mass flux conditions, Appl. Therm. Eng. 102 (2016) 391–401.
[44] X. Lei, H. Li, W. Zhang, N.T. DinhZ, Y. Guo, S. Yu, Experimental study on the difference of heat transfer characteristics between vertical and horizontal flows of supercritical pressure water, Appl. Therm. Eng. 113 (2017) 609–620.
[45] X. Zhu, Q. Bi, D. Yang, T. Cheng, An investigation on heat transfer characteristics of different pressure steam-water in vertical upward tube, Nucl. Eng. Des. 239 (2009) 381–388.
[46] S. Mokry, I. Pioro, A. Farah, K. King, S. Gupta, W. Peiman, P. Kirillov, Development of supercritical water heat-transfer correlation for vertical bare tubes, Nucl. Eng. Des. 241 (4) (2011) 1126–1136.
[47] F. Wang, Y. Yang, H. Gu, M. Zhao, H. Li, D. Lu, Experimental research on heat transfer performance of supercritical water in vertical tube, Atomic Energy Sci. Technol. 47 (2013) 934–939.
[48] S. Zhang, H. Gu, X. Cheng, Z. Xiong, Experimental study on heat transfer of supercritical Freon flowing upward in a circular tube, Nucl. Eng. Des. 280 (2014) 305–315.
[49] S. Zhang, Experimental and Fluid Scaling Studies on the Convective Heat Transfer of Supercritical Fluid Ph.D. thesis, School of Mechanical Engineering, Shanghai Jiaotong University, 2015.
[50] Y. Cui, H. Wang, Experimental study on convection heat transfer of R134a at supercritical pressures in a vertical tube for upward and downward flows, Appl. Therm. Eng. 129 (2018) 1414–1425.
[51] K. Kang, S. Chang, Experimental study on the heat transfer characteristics during the pressure transients under supercritical pressures, Int. J. Heat Mass Transf. 52 (2009) 4946–4955.
[52] X. Cheng, Y. Yang, S. Huang, A simplified method for heat transfer prediction of supercritical fluids in circular tubes, Ann. Nucl. Energy 36 (2009) 1120–1128.
[53] Y. Fan, G. Tang, X. Li, D. Yang, S. Wang, Correlation evaluation on circumferentially average heat transfer for supercritical carbon dioxide in non-uniform heating vertical tubes, Energy 170 (2019) 480–496.
[54] P. Jiang, Y. Zhang, R. Shi, Experimental and numerical investigation of convection heat transfer of CO_2 at supercritical pressures in a vertical mini-tube, Int. J. Heat Mass Transf. 521 (2008) 3052–3056.
[55] H. Zahlan, S. Tavoularis, D. Groeneveld, A look-up table for trans-critical heat transfer in water-cooled tubes, Nucl. Eng. Des. 285 (2015) 109–125.
[56] Y. Cui, Experimental Research on Heat Transfer Characteristics of Supercritical Pressure R134a in a Vertical Tube Master. thesis, School of Mechanical Engineering, Tianjin University, 2016.
[57] S.K. Dubey, R.P. Vedul, K.N. Iyer, A.J. Gaikwad, Local heat transfer coefficient measurements using thermal camera for upward flow of Freon 22 in a vertical tube at supercritical conditions and development of correlations, Nucl. Eng. Des. 328 (2018) 80–94.
[58] T. Yamashita, S. Yoshida, H. Mori, S. Morooka, H. Komita, K. Nishida, Heat transfer study under supercritical pressure conditions, in: Proceedings of the GENES4/ANP2003 International Conference on Global Environment and Advanced Nuclear Power Plants, 35, International Atomic Energy Agency, Kyoto, Japan, 2003.
[59] S. Koshizuka, N. Takano, Y. Oka, Numerical analysis of deterioration phenomena in heat transfer to supercritical water, Int. J. Heat Mass Transf. 38 (1995) 3077–3084.
[60] B.S. Shiralkar, P. Griffith, The Deterioration in Heat Transfer to Fluids at Supercritical Pressure and High Heat Fluxes, MIT Engineering Projects Laboratory, Cambridge, 1968 DSR-70332-55.
[61] W. Chen, X. Fang, A new heat transfer correlation for supercritical water flowing in vertical tubes, Int. J. Heat Mass Transf. 78 (2014) 156–160.
[62] Q. Zhang, H. Li, X. Lei, J. Zhang, X. Kong, Study on identification method of heat transfer deterioration of supercritical fluids in vertically heated tubes, Int. J. Heat Mass Transf. 127 (128) (2019) 674–686.
[63] B. Zhu, J. Xu, X. Wu, J. Xie, M. Li, Supercritical “boiling” number, a new parameter to distinguish two regimes of carbon dioxide heat transfer in tubes, Int. J. Therm. Sci. 136 (2019) 254–266.